ICETOOLS

REPORT 2025:1135





IceTools

Development of an improved model for assessment of snow and ice loads on overhead power lines

HANNA SABELSTRÖM, CHRISTOFFER HALLGREN

Foreword

Programmet Risk- och tillförlitlighetsanalys har initierat projektet IceTools – Utveckling av en modell för riskövervakning och tillförlitlighetsberäkning av is- och snöpåbyggnad på ledningar. Is- och snö på distributionsledningar kan leda till problem och skador på ledningar. Speciellt under de senaste vintrarna har stora tunga snöfall lett till flera strömavbrott och havererade ledningar.

Projekt har syftet att vidareutveckla och förbättra modellverktyget för att bättre kunna beräkna islaster och dimensionera kraftledningar i Sverige. Projektet har genomförts av PL Hanna Sabelström med kollegan Christoffer Hallgren.

Stort tack till programstyrelsen för deras engagemang i projektet:

- August Millqvist, Öresundskraft
- Carl Johan Wallnerström, Ei (adj)
- Emil Welin, Vattenfall Eldistribution
- Fredrik Andersson, Elinorr
- Fredrik Sjödin, Installatörsföretagen
- Geoffrey Jordaan, Svenska kraftnät
- Göran Sandström, Umeå Energi

- Hampus Halvarsson, Jämtkraft Elnät
- Henric Johansson, Jönköping Energi Nät
- Jenny Paulinder, Göteborg Energi Nät (ordförande)
- Linus Hansson, Ellevio
- Magnus Brodin, Skellefteå Kraft Elnät
- Niclas Eriksson, E.ON Energidistribution

Följande bolag har deltagit som intressenter till projektet. Energiforsk framför ett stort tack till samtliga för värdefulla insatser.

- Svenska kraftnät
- Ellevio AB
- Vattenfall Eldistribution
- E.ON Energidistribution
- Göteborg Energi Elnät
- Elinorr
- Jämtkraft Elnät
- Öresundskraft
- Skellefteå Kraft
- Umeå Energi
- Kraftringen Nät
- Jönköping Energi Nät

- PiteEnergi Elnät
- Karlstads El och Stadsnät
- Karlskoga Elnät
- Elinorr ekonomisk förening;
- Bergs Tingslags Elektriska
- Blåsjön Nät
- Dala Energi Elnät
- Elektra Nät
- Gävle Energi
- Hamra Besparingsskog
- Hofors Elverk

- Härjeåns Nät
- Härnösand Elnät
- Ljusdal Elnät
- Malungs Elnät
- Sandviken Energi Nät
- Sundsvall Elnät
- Söderhamn Elnät
- Åsele Elnät
- Årsunda Kraft & Belys.fören.
- Övik Energi Nät
- Ei (adjungerad)

Stockholm i oktober 2025

Susanne Stjernfeldt

Energiforsk AB

Forskningsområde Elnät Vindkraft och Solel

Här redovisas resultat och slutsatser från ett projekt inom ett forskningsprogram som drivs av Energiforsk. Det är rapportförfattaren/-författarna som ansvarar för innehållet.





Summary

This research project, funded by Energiforsk (Project EVU10155), addresses the challenges posed by snow and ice loads on power lines, which can lead to failures and power outages. The existing icing model, LineLoads, developed by Kjeller Vindteknikk and tailored for Norwegian conditions, has proven less reliable for Sweden's distribution network, which primarily traverses dense forests in lower terrain. To improve accuracy for Swedish conditions, a higher-resolution model has been developed, enhancing local terrain representation and spatial variability of the meteorological fields.

Wind data from the new model was compared with measurements from over 100 SMHI stations across Sweden, categorized by terrain types. The high-resolution model's wind data was long-term corrected using a longer time series generated with a model with coarser resolution. Both short and long periods were compared with SMHI wind observations. The comparison indicates that the new model is more precise with reduced wind speed bias, especially in terrain classes with low vegetation, permanent forests, and urban environments.

Additionally, a video recording and accompanying notes from Vattenfall Eldistribution, documenting weather conditions and loads on a distribution line at a forested location in Northern Sweden during the winter of 2017-2018, served as a baseline for validation. The time period covered by the recording was analyzed by examining temperature, wind speed, precipitation and ice load. The time evolution of meteorological conditions and ice load on the conductors and shield wires were compared with the output from the new model.

Analyzing the video recordings highlighted the importance of wind speed reduction due to local sheltering in forested terrain and revealed discrepancies both in the buildup and shedding phase of the icing events when comparing to the model predictions. Furthermore, the model's accuracy is sensitive to temperature, affecting melting predictions. The video analysis confirmed the stochastic nature of the ice shedding phenomenon. In several cases partly shedding occurred, leaving a layer of ice/snow on the conductors, whereas the model assumes complete shedding after melting periods or strong wind events. This further complicates the prediction of ice persistence and time evolution of ice load on the conductors during subsequent icing events.

While the validation exercises conducted in this project have given valuable insight into the main challenges in predicting ice loads on distribution lines in forested areas, long-term, direct or indirect measurements of ice load together with meteorological data would be required for a proper statistical calibration of the icing model.



Keywords

Ice load, weather modelling, icing model, distribution network, meteorology, cold climate, forested terrain, validation

Islast, nedisning, vädermodell, distributionsnät, skogsmiljö, meteorologi, kallt klimat, validering



Sammanfattning

Detta forskningsprojekt, finansierat av Energiforsk (Projekt EVU10155), behandlar utmaningarna med snö- och islaster på kraftledningar, vilket kan leda till driftsstörningar och strömavbrott. Den nuvarande modellen för nedisning, LineLoads, som är utvecklad av Kjeller Vindteknikk är anpassad för norska förhållanden och har visat sig vara mindre tillförlitlig för det svenska distributionsnätet, som ofta går genom tät skog i lägre terräng.

För att förbättra noggrannheten för svenska förhållanden har en modell med högre horisontell upplösning utvecklats, vilket bättre representerar lokal terräng och den rumsliga variationen i meteorologiska parametrar. Vinddata från den nya modellen har jämförts med mätningar från över 100 SMHI-stationer över hela Sverige, kategoriserade efter terrängtyp. Vinddata från modellen med hög upplösning långtidskorrigerades med hjälp av en längre tidsserie genererad med en modell med grövre upplösning. Både kort- och långtidsperioder jämfördes med SMHI:s vindobservationer. Jämförelsen visar att den nya modellen är mer exakt, med en minskad vindhastighetsbias, särskilt i terrängklasser med låg vegetation, permanent skog och urbana miljöer.

Som en del av valideringsarbetet har videomaterial och anteckningar från Vattenfall Eldistribution analyserats. Materialet dokumenterade väderförhållanden och snölaster på en distributionsledning i ett skogsområde i norra Sverige under vintern 2017–2018. Analysen omfattade en jämförelse mellan modell och observationer avseende temperatur, vindhastighet, nederbörd och islast.

Resultaten visar att lokal skärmning i skogsterräng påverkar vindhastigheten avsevärt, vilket i sin tur påverkar isbildningen. Avvikelser noterades både i uppbyggnads- och smältfasen av isbildningshändelserna. Modellens känslighet för temperatur har visat sig vara avgörande för att korrekt förutsäga smältning. Videoanalysen bekräftade också att snö- och issläpp från linan är ett stokastiskt fenomen. I flera fall skedde endast delvis snösläpp, vilket modellen inte tar hänsyn till då den antar en helt ren lina efter smältperioder eller kraftiga vind.

Projektet har identifierat flera viktiga utmaningar i modelleringen av islast på distributionsledningar i skog. För att uppnå en mer tillförlitlig statistisk kalibrering av modellen krävs dock ytterligare mätningar av islaster i kombination med meteorologiska data.



List of content

| 1 | Introd | ntroduction | | | |
|-------|---------|-------------|---|----|--|
| 2 | Data a | nd mod | del development | 12 | |
| | 2.1 | Model | l data | 12 | |
| | 2.2 | Statist | ical downscaling of meteorological variableS | 12 | |
| | 2.3 | The Li | The Line Loads model | | |
| 3 | Valida | tion wi | th wind observations | 15 | |
| | 3.1 | Observ | vational data | 15 | |
| | 3.2 | Compa | 15 | | |
| 4 | Valida | tion ag | ainst video recording of icing episodes | 21 | |
| | 4.1 | Compa | arison of LineLoads calculations with video recording | 21 | |
| | | 4.1.1 | Period 1: Fast growth | 23 | |
| | | 4.1.2 | Period 2: Very heavy loaded | 25 | |
| | | 4.1.3 | Period 3: Maximum load | 27 | |
| | | 4.1.4 | Period 4: Maximum load on left line | 29 | |
| | | 4.1.5 | Period 5: Growth | 31 | |
| | | 4.1.6 | Period 6: End of icing season | 33 | |
| 5 | Discus | sion | | 36 | |
| 6 | Conclu | ısion ar | nd recommendations | 38 | |
| 7 | Bibliog | graphy | | 39 | |
| Apper | ndix A | | Description of the KVTMeso model | 41 | |
| | A.1 | Model | l Setups | 41 | |
| | A.2 | Input | data | 43 | |
| Apper | ndix B | | Description of the icing calculations | 45 | |
| | | B.1.1 | Model for rime ice | 47 | |
| | | B.1.2 | Model for snow accretion | 52 | |
| Apper | ndix C | | Validation using SMHI observations | 56 | |



1 Introduction

This research project addresses the challenges posed by snow and ice loads on distribution lines, which can result in failures and power outages. An improved prediction of the ice loads can, practically, help the distribution net owners to be better prepared and to optimize measures to prevent these failures. In a broader perspective, a good understanding of the icing climatology is important when planning new distribution lines and when investing in existing ones.

An example of ice load on a distribution line is shown in Figure 1-1, where precipitation as wet snow has stuck to the lines and initiated the accumulation of snow on the conductors. Later, the snow sleeve has probably grown in size and weight due to accumulation of dry snow on top of the wet snow sleeve. In this report, we use the term "ice load" to describe any type of snow or ice accreted on the power line phase conductors or shield wires. Typically, the ice load grows symmetrically outward from the line, forming a cylindrical shape that eventually becomes so heavy that it may cause line failure. Even if the line does not collapse, it is problematic to have low-hanging lines violating the ground clearance requirements. And lastly, sudden ice shedding may cause conductor jumping and high amplitude oscillations which can often lead to electrical failures.



Figure 1-1. Example of ice load on a distribution line in Northern Sweden. Picture received from Vattenfall Eldistribution (included with permission).



Over the years, Kjeller Vindteknikk (KVT) has developed an icing model for power lines, known as LineLoads, primarily tailored to Norwegian conditions characterized by exposed mountainous or maritime areas and high wind speeds. However, this model has proven less reliable for Sweden's distribution network, which predominantly traverses forested areas in lower terrain. The largest issues seem to occur for lines in sheltered forests in the northern half of Sweden where snow is allowed to persist on the lines for extended periods without any wind that removes the snow. This project aims to enhance the accuracy of LineLoads calculations for Swedish conditions.

A precondition for a successful prediction of icing on power lines is meteorological data of sufficient quality to represent local conditions. To achieve this, a model with higher horizontal resolution (750 m \times 750 m) has been developed to better represent the local terrain and its importance for ice-buildup. The model has been run for all of Sweden with a temporal resolution of one hour. A description of the model and the implementation in the LineLoads calculations are presented in Chapter 2.

A challenge with models is to validate them towards real-case scenarios. For the icing model this is particularly difficult due to the lack of measurements of wind and concurrent icing in the terrain of interest. As validation of the model run presented in this report, comparisons have been made to available wind data from meteorological weather stations. Wind data from the model have been compared with observations from over 100 SMHI measurement stations across Sweden. The stations have, in addition, been categorized into different types of terrain depending on the surroundings of each weather station. The high-resolution model's wind data have been long-term corrected using the longer time series with a 3 km x 3 km horizontal resolution. Both short- and long-term time periods have been compared to wind observations from SMHI. This comparison is described in Chapter 3.

In addition, a video recording and accompanying notes received from Vattenfall Eldistribution, has served as a baseline for validation of the icing model. From the video recordings, qualitative information can be derived on weather conditions and loads on a specific distribution line in forested terrain in Northern Sweden during the winter of 2017-2018. In chapter four, the video analyses are compared to the model results. This validation includes comparing the timing and duration of icing along with the modelled temperature, wind speed, precipitation.



2 Data and model development

2.1 MODEL DATA

Calculations of ice loads are based on meteorological data available in the KVTMeso product suite. The main dataset is a low-resolution dataset of 3 km x 3 km horizontal resolution (KVTMeso3) and 1 h temporal resolution extending from 1979 till present. In addition, wind speeds and cloud liquid water content (LWC) from simulations with high-resolution datasets are applied to downscale the wind and in-cloud icing to finer resolution. Two simulations are used for downscaling the KVTMeso3 wind speeds; an older simulation of 1 km x 1 km horizontal resolution (KVTMeso1) and the new simulation in 750 m x 750 m horizontal resolution generated for this analysis (KVTMeso750). In addition, the new model, KVTMeso750, is used to downscale the cloud LWC. The KVTMeso product suite and the datasets involved are described in further detail in Appendix A.

2.2 STATISTICAL DOWNSCALING OF METEOROLOGICAL VARIABLES

The fine scale model wind series are used to refine reference wind series on hourly basis with a quantile regression technique (QQ). Further information on the methodology can be found in (Liléo, Berge, Undheim, Klinkert, & Bredesen, 2013) (in which it is described as the U&N method). In this analysis the KVTMeso3 dataset is used as the primary reference data. Wind speed and wind direction are treated separately in the method.

The wind direction adjustment is carried out by first identifying the difference in the prevailing wind direction between the fine scale data and the reference data. The concurrent data are then adjusted in accordance with the wind direction difference and sorted individually in ascending order. The wind direction adjustment to be applied is found by looking at the difference between the sorted datasets using a QQ-approach.

In the wind speed adjustment, the sorted wind directions are divided into 12 sectors in such a way that they all contain the same amount of data. The wind speeds in each of the 12 sectors are sorted individually for the fine scale data and for the reference data to find wind speed adjustment functions. To extrapolate velocities outside the range of simultaneous data a regression line is made based on the 20 % highest data. This regression line is used as a function for extrapolating the 10 % highest velocities captured in the dataset of simultaneous values.

If the simultaneous dataset contains few samples, or any of the datasets contain extreme outliers the extrapolation may create unphysically large wind speeds. To avoid this, the trend line is not used for extrapolation beyond the highest velocity in the simultaneous data; the extrapolation is instead done by following a line of constant ratio, corresponding to the difference of the highest value of the trend line at the highest value in the reference data of the simultaneous data (i.e. following the 1:1 line from the upper-most reference wind speed in the simultaneous data).



This methodology is consistent in the manner that both the distribution of the velocity and the wind direction in the corrected timeseries (or synthesized timeseries) will be the same as for the original observed timeseries in the concurrent period, although the timing can be different. The accuracy of the timing will depend on the correlation between the fine scale data and reference data.

In-cloud icing (also referred to as rime icing) occurs when supercooled cloud or fog droplets present in the air collide with an object exposed to it. The phenomenon rarely causes any great loads in low and sheltered areas, however a thin layer of rime ice on the conductors may trigger further growth through accumulation of snow, either dry or wet. To have the best possible representation of local rime icing conditions, the cloud LWC is statistically downscaled utilizing a multiple linear regression model, optimized on the two datasets.

2.3 THE LINE LOADS MODEL

The LineLoads model is a tool developed by KVT to calculate the climatic loads (wind and ice) for planning and design of power lines according to the European standard (EN50341-1 (EN 50341 - 1: Overhead electrical lines exceeding AC 1 kV - Part 1: General requirements - Common specifications, 2012)). The LineLoads model integrates physical models for various types of icing and wind data and results in a long-term time series of wind and ice conditions at a specific location. The time series is then used to statistically derive different return values of wind and ice loads, as well as their combinations. Below are the main meteorological variables incorporated in the model that affect icing conditions (for further details, see Appendix B).

- In-cloud icing occurs when supercooled cloud droplets collide with objects tall enough to penetrate the cloud base, forming rime ice upon impact. This phenomenon is most common in hilly or mountainous regions and intensifies with altitude.
- Wet snow accumulates on overhead power lines during snowfall at temperatures just above freezing. The accumulation rate increases with wind speed, particularly the wind component perpendicular to the line direction. Wet snow accumulation is calculated using an ensemble methodology to expand the statistical basis, involving 40 different model runs with slight temperature perturbations. The model also includes processes like melting, sublimation, and ice shedding to account for the reduction or removal of wet snow.
- Dry snow tends to accumulate on power lines already covered by ice or
 wet snow, typically during calm wind periods following wet snow or rime
 episodes. This is most pronounced in areas with generally calm winds
 close to the ground. In Sweden, combinations of rime icing and dry snow
 are crucial for extreme value distribution, even at elevations as low as 200
 meters above sea level.



- Temperature and relative humidity conditions are crucial. As soon as the temperature rises above 0°C, melting occurs rapidly, and dry air leads to sublimation.
- **High wind speeds** can cause vibrations in the lines and affect the buildup of snow on the power lines during snowfall. Wind gusts are parameterized in the model using the modeled turbulent kinetic energy.



3 Validation with wind observations

3.1 OBSERVATIONAL DATA

The 10-m model wind data, calculated using interpolation between the model's vertical levels, from the KVTMeso750 and KVTMeso1 models has been compared to 10-m observed hourly averages of wind data available in the archive of the Swedish Meteorological and Hydrological Institute (SMHI). All available observation stations that are active and lie within the model domains of the models, having a measurement period of at least 5 years and are overlapping in time with the time-period that is directly simulated by the KVTMeso750 model are included. However, observations with a data record of a resolution lower than 0.5 m/s are not included in the analysis. This results in a data set of in total 132 observation sites, spread across all of Sweden (see Appendix C).

The SMHI observation sites are divided into five different terrain categories following a slightly modified version of the Eurocode 1 EN1991-1-4 Annex A, and by manual inspection of satellite images for each observation location. The terrain categories are presented in Table 3-1.

Table 3-1: Terrain categories based on the Eurocode standard.

| Terrain category | Description |
|------------------|--|
| 0 | Sea, coastal area |
| 1 | Lake, field, mountain terrain without obstacles and low local complexity |
| 2 | Low vegetation with only a few obstacles or buildings |
| 3 | Permanent forest, villages |
| 4 | Urban |

In total, 28 of the SMHI stations were classified as located in terrain category 0; 13 in terrain category 1; 69 in terrain category 2; 20 in terrain category 3; and 2 in terrain category 4. An overview of the stations and their respective terrain category is provided in Appendix C.

Further, the SMHI data was reduced to only cover the time-period October 1 to May 31 for each year and only data that was non-zero and controlled and approved in the quality control by SMHI is used in the analysis.

3.2 COMPARISON BETWEEN MODEL DATA AND OBSERVATIONS

For all stations in the analysis, the 10-m wind speeds from the KVTMeso750 model have been compared to the overlapping data from the SMHI observations. On average, there was a positive bias in the model of 1.03 m/s and an RMSE of 2.11 m/s. The coefficient of determination, the R2 value, was on average 0.58 for the hourly data (0.77 for 24-hour averages). In Figure 3-1, the wind speed and wind direction time-series from the KVTMeso750 model and the SMHI observations for the overlapping time-period is shown for one of the stations in the inland of northern Sweden. In Figure 3-2, scatter plots of wind speed and wind direction extracted from this time-series is shown for the same station.



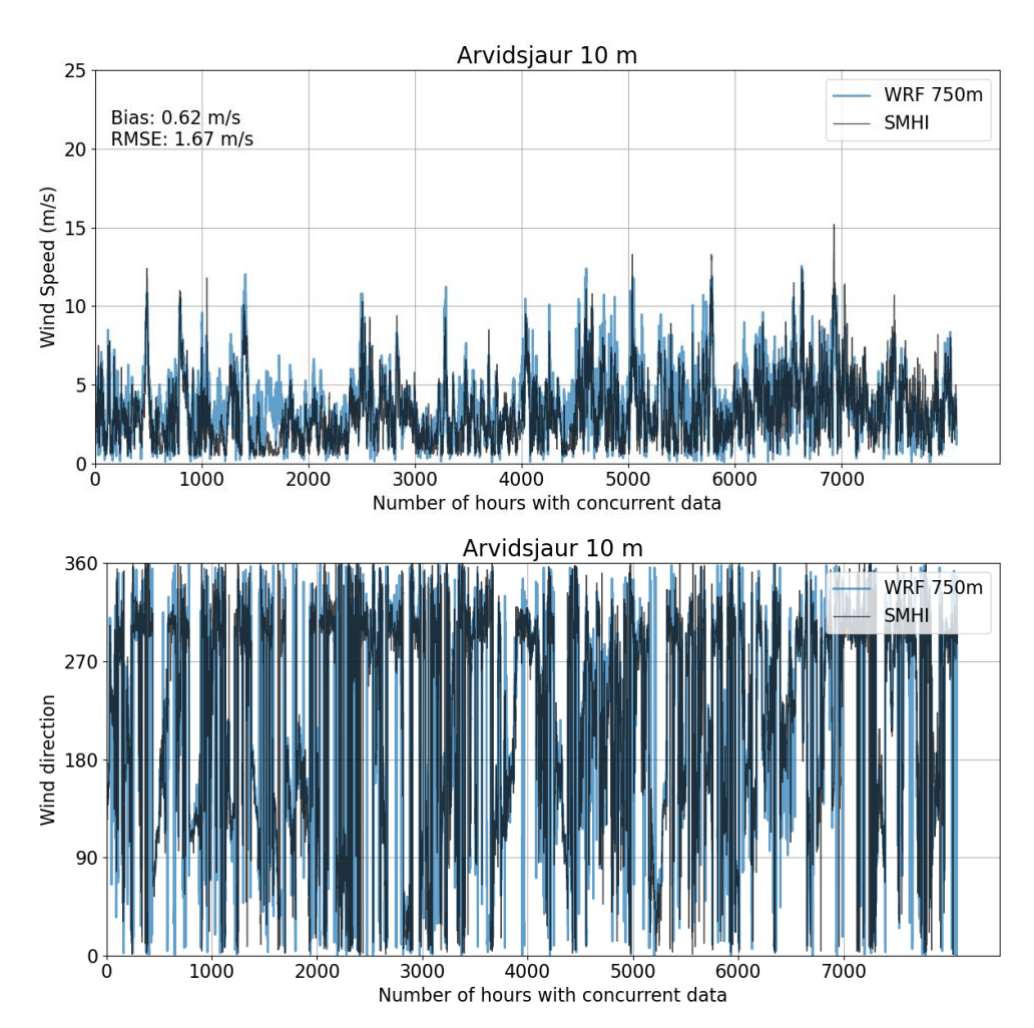


Figure 3-1: Example from Arvidsjaur of time-series of wind speed (above) and wind direction (below) for the overlapping time-period with data in the KVTMeso750 model and in SMHI observations.

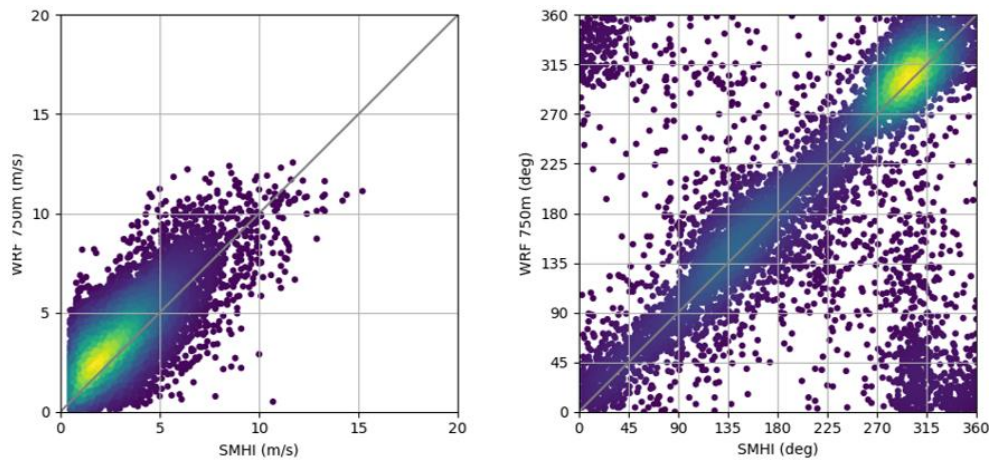


Figure 3-2: Example from Arvidsjaur of scatter plots of wind speed (left) and wind direction (right) for the overlapping time-period with data in the KVTMeso750 model and in SMHI observations.

Using the long-term correction method, synthesised time-series of hourly wind data have been generated covering a period from September 1, 1979, until August



31, 2024, from both the KVTMeso750 and the KVTMeso1 models, using the long-term data set from the KVTMeso3 model. The generated long-term data sets have been compared with the overlapping period (October to May) for the SMHI stations, which vary between different stations depending on the data availability in the observations.

In Figure 3-3 and Figure 3-4 the distributions of wind speed and wind direction are visualized for one of the sites in the analysis. In this specific case, Figure 3-3, the wind speed distribution from the synthesised KVTMeso750 and the KVTMeso1 models follow each other up to 10 m/s, with only small improvements in the KVTMeso750 model. In wind speeds over 10 m/s, the KVTMeso750 model clearly performs better than the KVTMeso1 model. For this site, only small changes are seen in the distribution of wind direction, Figure 3-4. The KVTMeso750 model better picks up the SE and NW flow, which is seen in the observations, while the KVTMeso1 model has a more even spread between wind directions, apart from the dominant NW sector. In general, it seems that the wind direction distribution at sites more exposed to sheltering are slightly better resolved in KVTMeso750 than in KVTMeso1.

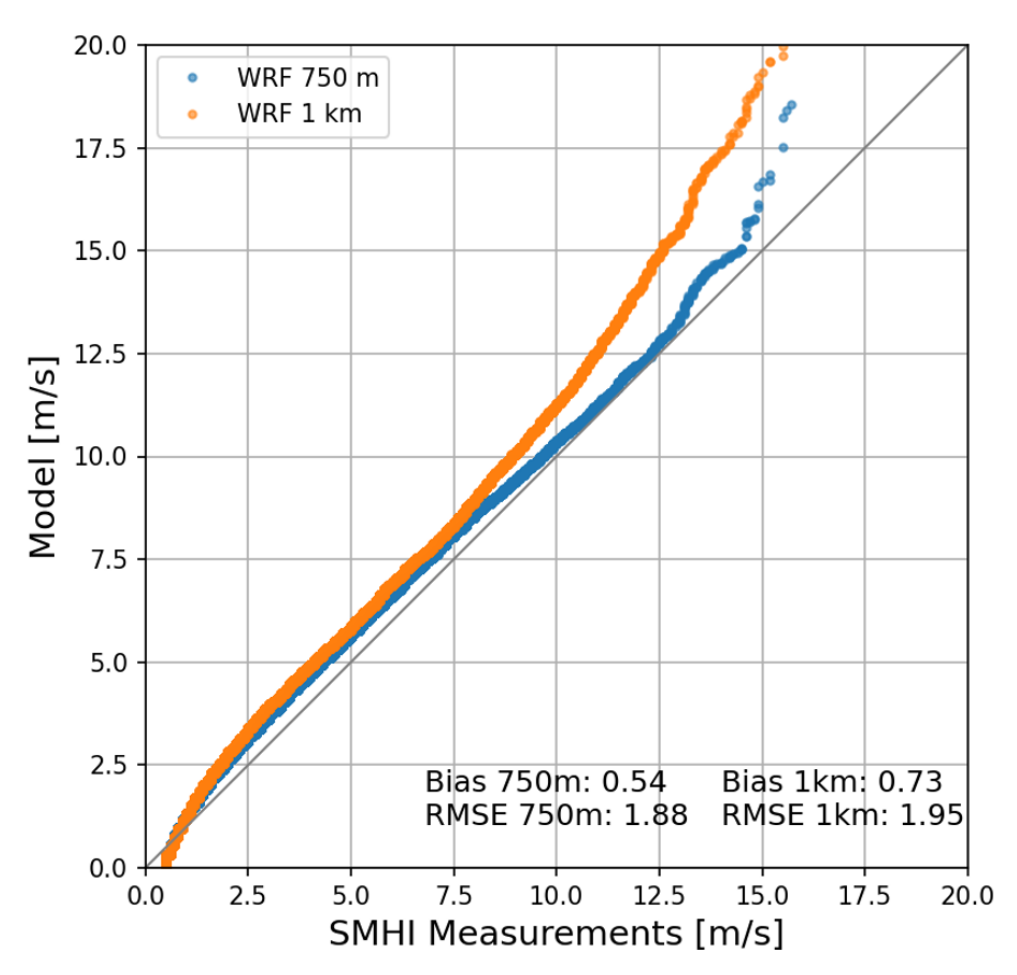


Figure 3-3: Example from Arvidsjaur of a QQ-plot for the synthesised wind speed data generated using the KVTMeso750 model (blue) and the KVTMeso1 model (orange) as compared to the SMHI measurements.



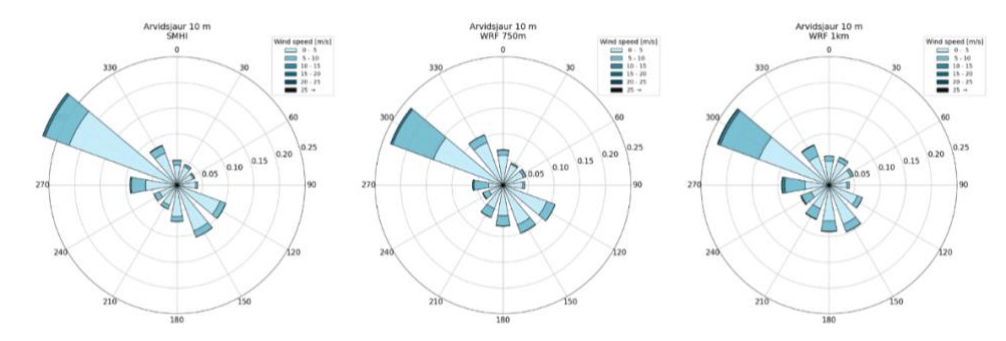


Figure 3-4: Example from Arvidsjaur of wind roses from the overlapping period of observations and synthesised model data showing the observations (left), output from the synthesised KVTMeso750 model (middle) and output from the synthesised KVTMeso1 model (right).

Comparing the results of the long-term corrected KVTMeso750 model to the results of the long-term corrected KVTMeso1 model, the long-term corrected KVTMeso750 model in general shows a smaller absolute value in bias, see Figure 3-5. For the long-term period, the bias for KVTMeso750 was on average 0.87 m/s while for KVTMeso1 it was 1.19 m/s. Also, the RMSE was lowered, from on average 2.50 m/s for KVTMeso1 to 2.25 m/s for KVTMeso750. In Table 3-1 the bias and RMSE for the different terrain classes are presented. The bias is improved for all terrain classes, except for category 1 where the absolute value of the bias for KVTMeso1 was lower. The larges improvement was in category 2, with an improvement of 34%. Similarly, RMSE was improved in all terrain categories except in category 1.



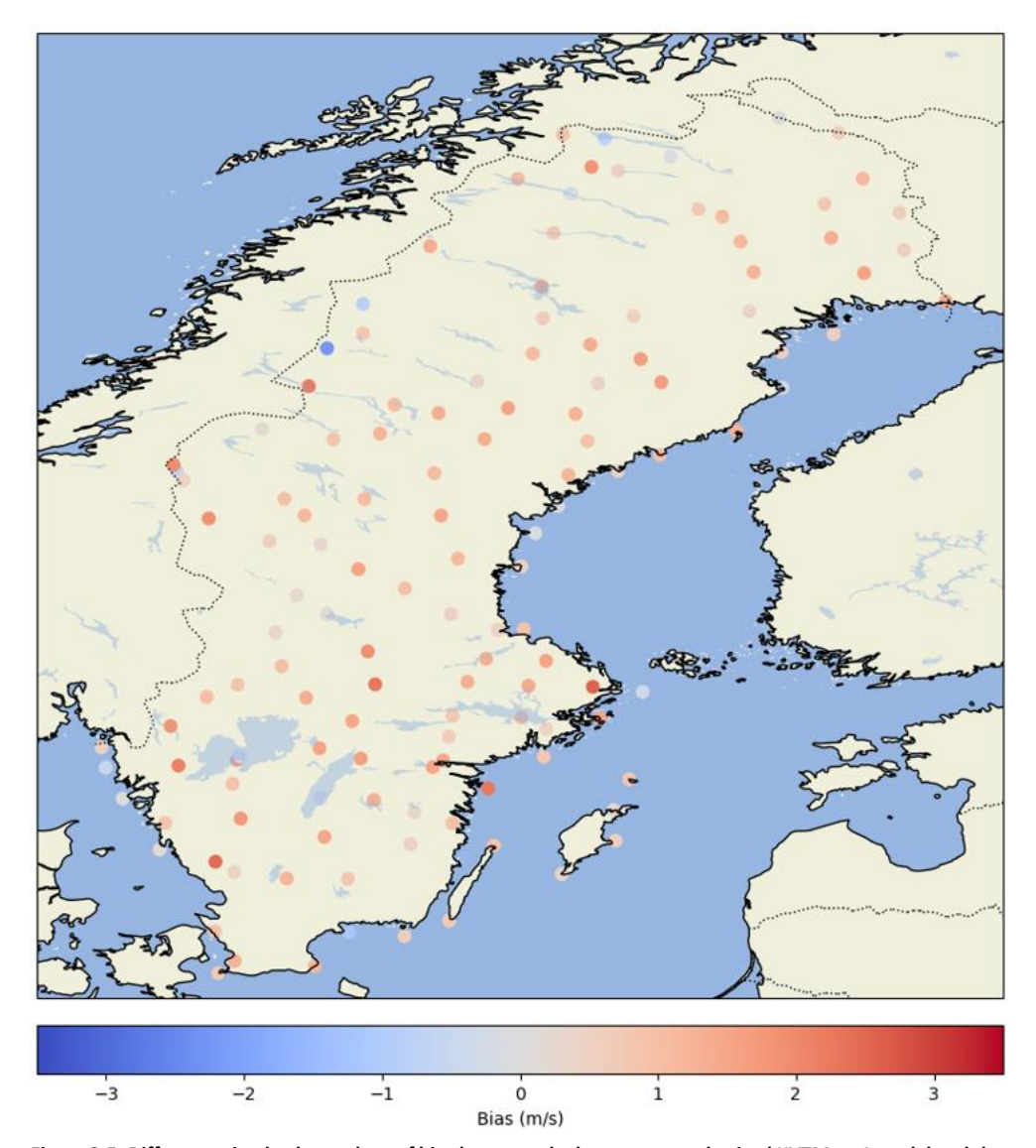


Figure 3-5: Differences in absolute values of bias between the long-term synthesised KVTMeso1 model and the long-term synthesised KVTMeso750 model, |bias1km|-|bias750m|, using the SMHI observations as reference.

Table 3-2: Bias and RMSE for the different terrain classes for the synthesised KVTMeso750 model and the synthesised KVTMeso1 model.

| Terrain category | Bias KVTMeso750 model [m/s] | Bias KVTMeso1 model [m/s] | RMSE KVTMeso750 model [m/s] | RMSE KVTMeso1 model [m/s] |
|---------------------|-----------------------------------|---------------------------------|-----------------------------------|---------------------------------|
| 0 | 0.43 | 0.53 | 2.39 | 2.44 |
| 1 | 0.25 | -0.15 | 3.07 | 3.03 |
| 2 | 1.06 | 1.59 | 2.04 | 2.43 |
| 3 | 1.26 | 1.59 | 2.29 | 2.48 |
| 4 | 1.18 | 1.49 | 1.93 | 2.11 |



4 Validation against video recording of icing episodes

A video recording showing a distribution line span in northern Sweden, close to Jokkmokk, has been shared by Vattenfall Eldistribution. The recording shows the ice build-up of the specific line section, located in a forest, during the winter episode from November 2017 to April 2018. In Figure 4-1, a snapshot from the recording is shown. The material has previously been analysed by Vattenfall Eldistribution and presented with daily values in a table indicating date, amount and type of precipitation, temperature and comments regarding relative humidity, a general comment on the icing load, and estimated level of ice/snow on the lines (on a scale from 0 to 3).



Figure 4-1: A video still from the analysed video recordings, showing the ice build-up on a span in a forest close to Jokkmokk.

4.1 COMPARISON OF LINELOADS CALCULATIONS WITH VIDEO RECORDING

A LineLoads calculation has been performed for the location of the span in the video recording. The data from the nearest grid point for KVTMeso3 model and for KVTMeso750 model have been extracted and used in the calculations. The high-resolution data from KVT750 model is used for statistical scaling of wind speed and in-cloud icing in the longer time series of KVTMeso3. In the comparison with the video recording both the long term time series (KVTMeso3 downscaled with KVTMeso750) and short term time series (KVTMeso750 only) are used. In addition, a scaling of the wind speed has been made based on experience of over-estimation of wind speed for lines located in and sheltered by forest and a reduction factor of 0.6 has been applied to the output wind speed. The outcome from the LineLoads



calculation is a time series of ice load (kg/m), wind speed, temperature and precipitation which is then compared to the video recording.

Figure 4-2 shows the results of the LineLoads calculations based on the KVTMeso750 model with and without the reduction factor for the wind speed for the time interval covered by the video recordings, November 2017 to end of March 2018. By reducing the wind speed, higher ice load is obtained, since more dry snow is allowed to accumulate on the line (illustrated by circles in the figure). In the model there is a function that triggers complete ice shedding when the wind speed reaches a certain level and the ice density is sufficiently low. The effect of this shedding is marked by arrows in the figure, for the case with reduced wind speeds no shedding due to wind speed is occurring. In further comparison with the video recording, the case with reduced wind speed is used.

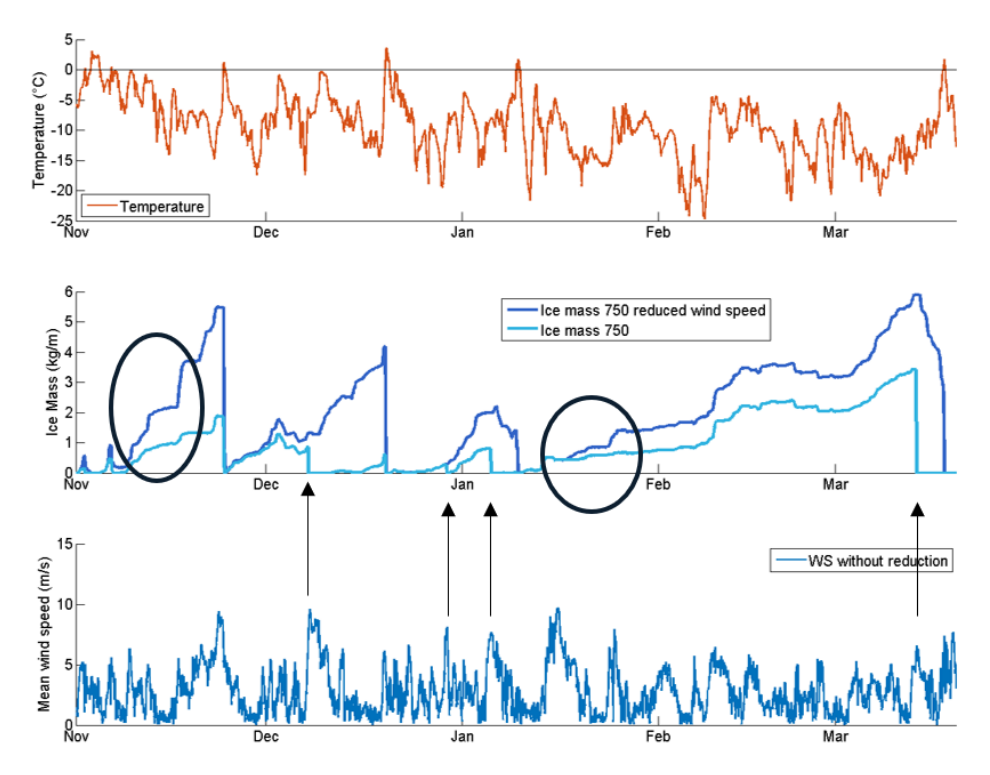


Figure 4-2: Results from the LineLoads model based on KVTMeso750 with and without reduction factor of the wind speed. The circles indicate occasions where the reduced wind speed results in larger growth of snow build-up during snow fall. The arrows indicate four occasions when snow is shredded off the line due to high wind speed. In the case of reduced wind speed, the threshold for this type of shedding is not reached, and ice load remains.

In the analysis of the video recording provided by Vattenfall Eldistribution, five different icing periods had been identified. These periods, plus an additional period at the end, have been used as basis for the comparisons of model data and video recording. In Figure 4-3, the time series of hourly data of temperature, ice mass, precipitation and mean wind speed from the model is plotted with the six different time periods marked. The comparison of model data and the video recording is described for each period in sections 4.1.1 to 4.1.6.



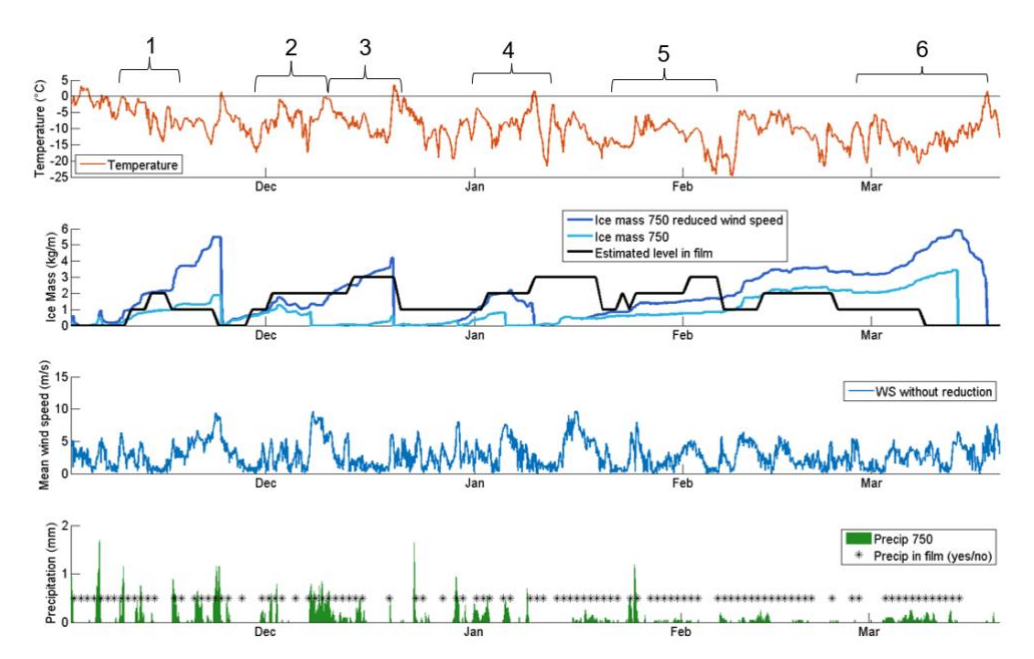


Figure 4-3: Results from the LineLoads model based on KVTMeso750. Notes from the video recording regarding the estimated level of icing and whether there was precipitation or not, are also included in the figure. The six time periods that are analysed further in the report are marked at the top of the figure.

4.1.1 Period 1: Fast growth

The first period, November 10th to November 19th, is classified by "fast icing growth" in the documentation of the video recording. The estimated level of ice increases from 0 to 2 during the period. The model results show an increased ice mass due to snow fall. The ice mass is higher for the high-resolution model (750) compared to the downscaled low-resolution model (750 LT). The period is shown in more detail in Figure 4-4 with the major events, A, B and C, described below. Figure 4-5 shows four video stills captured from the recording during the observed period.



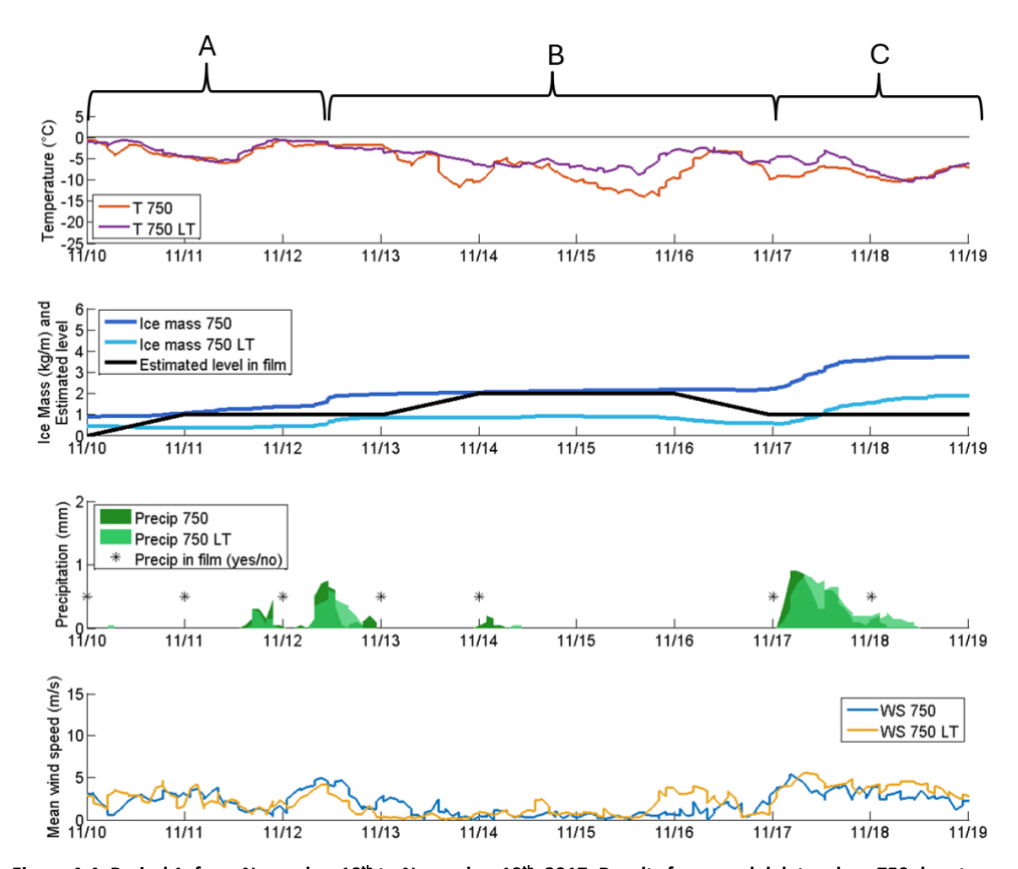


Figure 4-4: Period 1, from November 10th to November 19th, 2017. Results from model data where 750 denotes the high-resolution model (KVTMeso 750) and 750 LT is the downscaled courser resolution model (KVTMeso 3 downscaled by KVTMeso 750). Added are also noted estimated level of ice (0 to 3) and snow fall from the video recording documentation.

A: Minor ice accumulation was observed in the model data, with snowfall on the 12th accelerating the growth. The video recording indicates a minor ice load, and on the 12th, the snow appears to adhere, causing the lines to become heavier (level 1).

B: No ice growth was observed in the model. The video recording shows ice accumulation on the 14^{th} following the snowfall (level increased to 2). Oscillations of lines were noted on the 15^{th} and 16^{th}

C: Ice growth in model is observed between the 17th and 18th due to snowfall. The recordings shows partial shedding of snow on the morning of the 17th, possibly influenced by the wind.





Figure 4-5 Four video stills taken from the recordings during Period 1 to illustrate major events

4.1.2 Period 2: Very heavy loaded

The second period, December 1st to December 11th, is classified by "very heavy loaded" in the documentation of the video recording. The estimated level of ice increases from 1 to 2 during the period. The model results show an increased ice mass due to snow fall. The ice mass is higher for the high-resolution model (750) compared to the downscaled low-resolution model (750 LT). The period is shown in more detail in Figure 4-4 with the major events, A, B and C, described below. Figure 4-5 shows four video stills captured from the recording during the observed period.



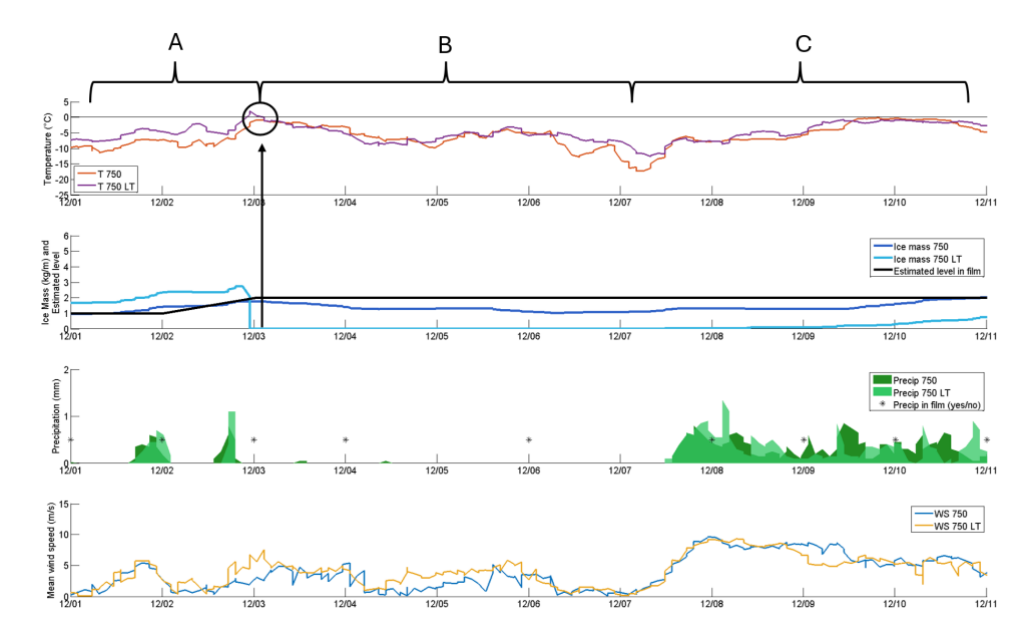


Figure 4-6: Period 2, from December 1st to December 11th, 2017. Results from model data where 750 denotes the high-resolution model (KVTMeso 750) and 750 LT is the downscaled courser resolution model (KVTMeso 3 downscaled by KVTMeso 750). Added are also noted estimated level of ice (0 to 3) and snow fall from the video recording documentation.

A: Ice growth is observed in the model due to snowfall. The 750 LT model shows melting as the temperature exceeds 0°C, as marked by the arrow. The video recording indicates snow accumulation during the period and no shedding at midnight.

B: No ice load is observed for the 750 LT model while sublimation occurs in the 750 model. The video recording shows no growth and the lines swing significantly on the 6^{th} .

C: Snowfall is observed in the model, but there is not much accumulation due to rather windy conditions. Small ice growth is observed in the model from the 10^{th} to the 11^{th} . The video recording shows heavy snowfall on the 9^{th} , with fog from the 8^{th} to the 10^{th} causing poor visibility. There was increased weight on the lines on the 10^{th} .





Figure 4-7 Four video stills taken from the recordings during Period 2 to illustrate major events

4.1.3 Period 3: Maximum load

The third period, December 10th to December 21st, is classified by "maximum load" in the documentation of the video recording. The estimated level of ice increases from 2 to 3 during the period. The model results show an increased ice mass due to snow fall and a complete shedding due to temperature at the end of the period. The ice mass is higher for the high-resolution model (750) compared to the downscaled low-resolution model (750 LT). The period is shown in more detail in Figure 4-8 with the major events, A, B and C, described below. Figure 4-9 shows four video stills captured from the recording during the observed period.



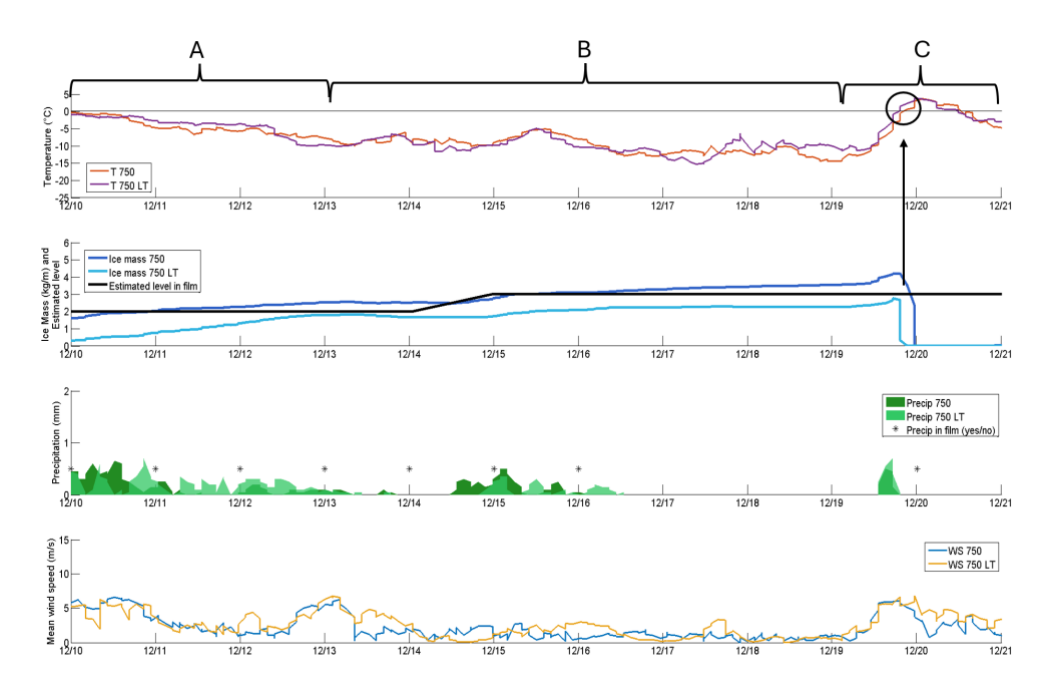


Figure 4-8: Period 3, from December 10th to December 21st, 2017. Results from model data where750 denotes the high-resolution model (KVTMeso750) and 750 LT is the downscaled courser resolution model (KVTMeso3 downscaled by KVTMeso750). Added are also noted estimated level of ice (0 to3) and snow fall from the video recording documentation.

A: Small ice growth is observed in the model. The video recording shows snow accumulation with increasing intensity on the $13^{\rm th}$

B: Growth is observed in the model on the 15^{th} , with continued growth until the 20^{th} . The video recording shows a heavy load on the right line on the 14^{th} , maintaining a high level until the 20^{th} .

C: The temperature rises above 0° C on the 20^{th} , resetting the ice load to zero (marked by arrow). The video recording shows a heavy load until the 20^{th} , with a snow drop (complete shedding) on the right and middle lines in the morning as the temperature increased from -25°C to 0.4° C. Snow remains on the left line.





Figure 4-9: Four video stills taken from the recordings during Period 3 to illustrate major events

4.1.4 Period 4: Maximum load on left line

The fourth period, January 1st to January 17th, is classified by "maximum load on left line" in the documentation of the video recording. The estimated level of ice increases from 1 to 3 during the period. The model results show an increased ice mass due to snow fall up to the 6th of January. On the 10th of January, a complete shedding occurs due to rising temperature. Up to this event the ice mass is higher for the high-resolution model (750) compared to the downscaled low-resolution model (750 LT). The period is shown in more detail in Figure 4-10 with the major events, A, B, C and D, described below. Figure 4-11 shows four video stills captured from the recording during the observed period.



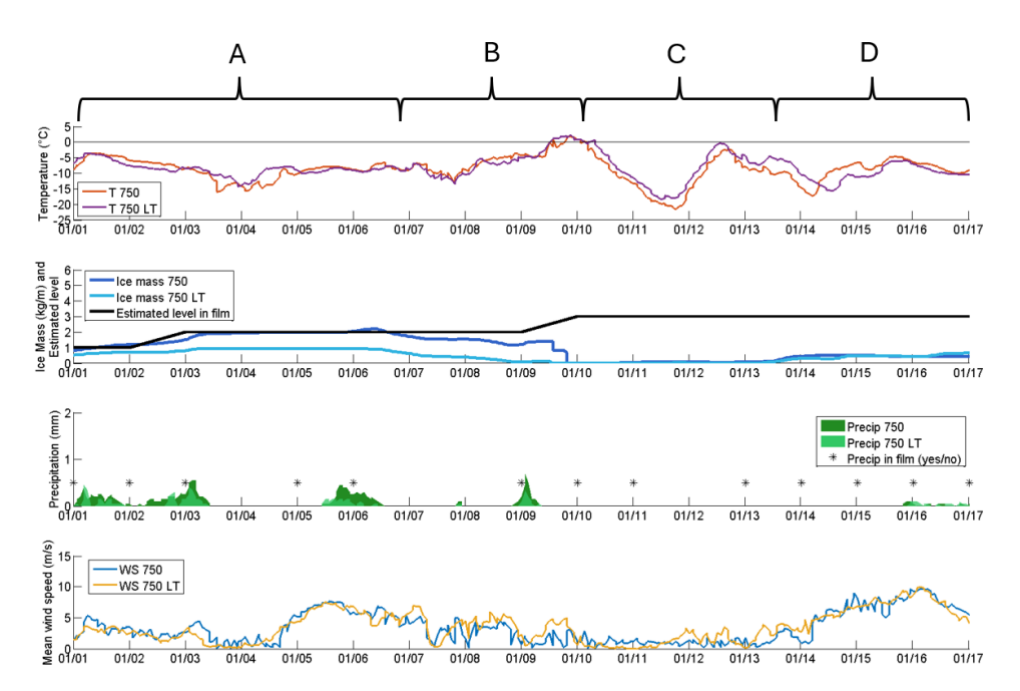


Figure 4-10: Period 4, from January 1st to January 17th, 2018. Results from model data where 750 denotes the high-resolution model (KVTMeso 750) and 750 LT is the downscaled courser resolution model (KVTMeso 3 downscaled by KVTMeso 750). Added are also noted estimated level of ice (0 to 3) and snow fall from the video recording documentation.

A: Small ice growth is observed in the model on the 3rd due to snowfall. The video recording shows snow accumulation, with the left line starting to become heavy on the 5th.

B: Sublimation is observed in the model, followed by melting with the temperature rising above 0°C on the 9th, resulting in no ice load. The video recording shows continued snow accumulation, with the left line becoming very heavy.

C: No growth is observed in the model. The video recording shows small accumulation, with the left line becoming very heavy.

D: Small growth is observed in the model. The video recording shows snow dropping from the left line (complete shedding) on the 15th, but not from the others (partial shedding on middle line).





Figure 4-11: Four video stills taken from the recordings during Period 4 to illustrate major events

4.1.5 Period 5: Growth

The fifth period, January 23rd to February 8th, is classified by "growth" in the documentation of the video recording. The estimated level of ice increases from 1 to 3 and then decreases to 1 during the period. The model results show a small increase in ice mass throughout the period. The ice mass for the high-resolution model (750) is on same level as the downscaled low-resolution model (750 LT). The period is shown in more detail in Figure 4-12 with the major events, A, B and C, described below. Figure 4-13 shows four video stills captured from the recording during the observed period.



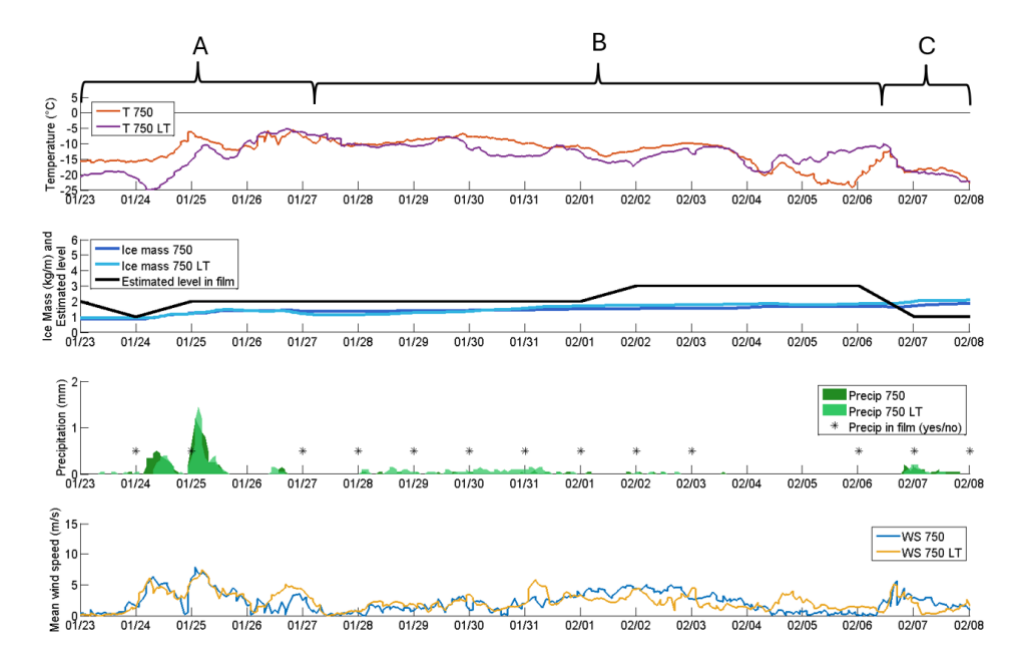


Figure 4-12: Period 5, from January 23rd to February 8th, 2018. Results from model data where750 denotes the high-resolution model (KVTMeso750) and 750 LT is the downscaled courser resolution model (KVTMeso3 downscaled by KVTMeso750). Added are also noted estimated level of ice (0 to 3) and snow fall from the video recording documentation.

A: Small ice growth is observed in the model around the 25th. The video recording shows some snow dropping from the right line on the 24th (wind observed at treetops) and from the left line on the 25th. Some snowfall on the 24th and 25th, resulting in increased load...

B: Hardly any change in ice load is observed in the model. The video recording shows no changes until the 2^{nd} , when the load increased due to snowfall.

C: A small increase in ice load is observed in the model. The video recording shows some swinging of lines and snow dropping on the 7th.





Figure 4-13: Four video stills taken from the recordings during Period 5 to illustrate major events

4.1.6 Period 6: End of icing season

The sixth period, March 1st to March 20th, illustrates the end of the icing season. This is the period where the largest deviations occur between the model and the observations, most likely due to the impact of solar radiation on ice shedding and melting that is not captured well enough in the model. The estimated level of ice decreases from 1 to 0 during the period. The model results show an increase of ice mass until the 14th of March when it decreases (due to sublimation) until temperature exceeds 0°C and a complete ice shedding takes place. The ice mass for the high-resolution model (750) is slightly higher than the downscaled low-resolution model (750 LT). The period is shown in more detail in Figure 4-14 with the major events, A, B and C, described below. Figure 4-15 shows four video stills captured from the recording during the observed period.



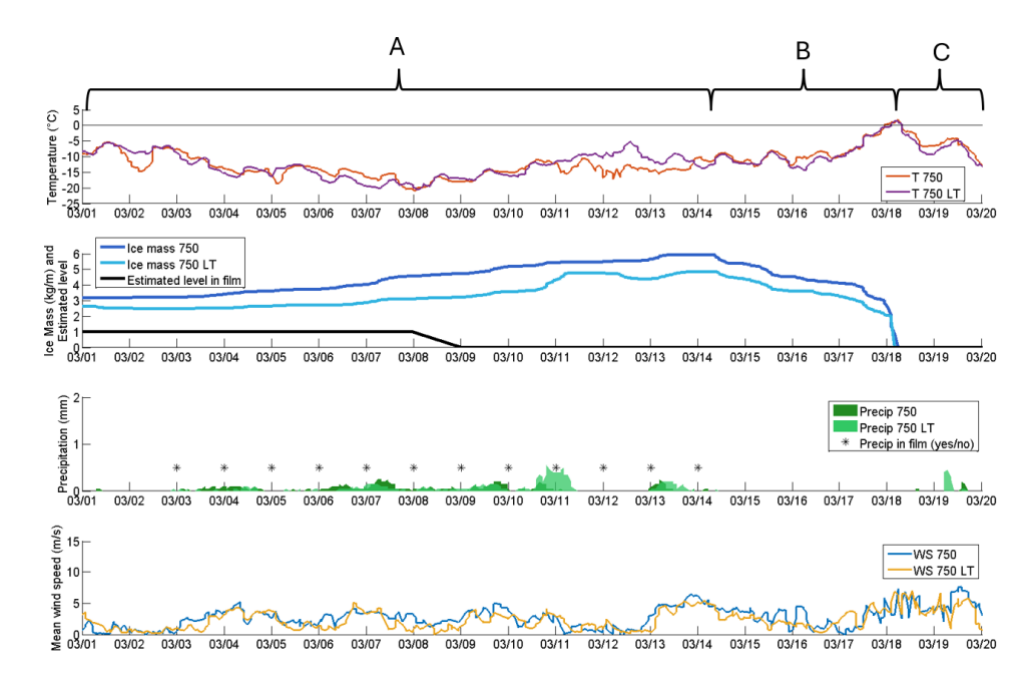


Figure 4-14: Period 6, from March 1st to March 20th, 2018. Results from model data where 750 denotes the high-resolution model (KVTMeso 750) and 750 LT is the downscaled courser resolution model (KVTMeso 3 downscaled by KVTMeso 750). Added are also noted estimated level of ice (0 to 3) and snow fall from the video recording documentation.

A: Small ice growth is observed in the model until the 14th. The video recording shows an unchanged load, with accumulation due to snowfall on the 4th. Snowfall on the 9th led to snow accumulation, followed by a snow drop (complete shedding). Some snow accumulation occurred during the nights, with oscillations during the daytime. The days were sunny.

B: A decrease in ice load was observed due to sublimation. The video recording shows sunny days with some variable line sag during daytime.

C: The temperature rose above 0°C, resetting the load to zero. The video recording shows that the magnitude of line sag decreased on the 18th, with the load disappearing after the 19th.



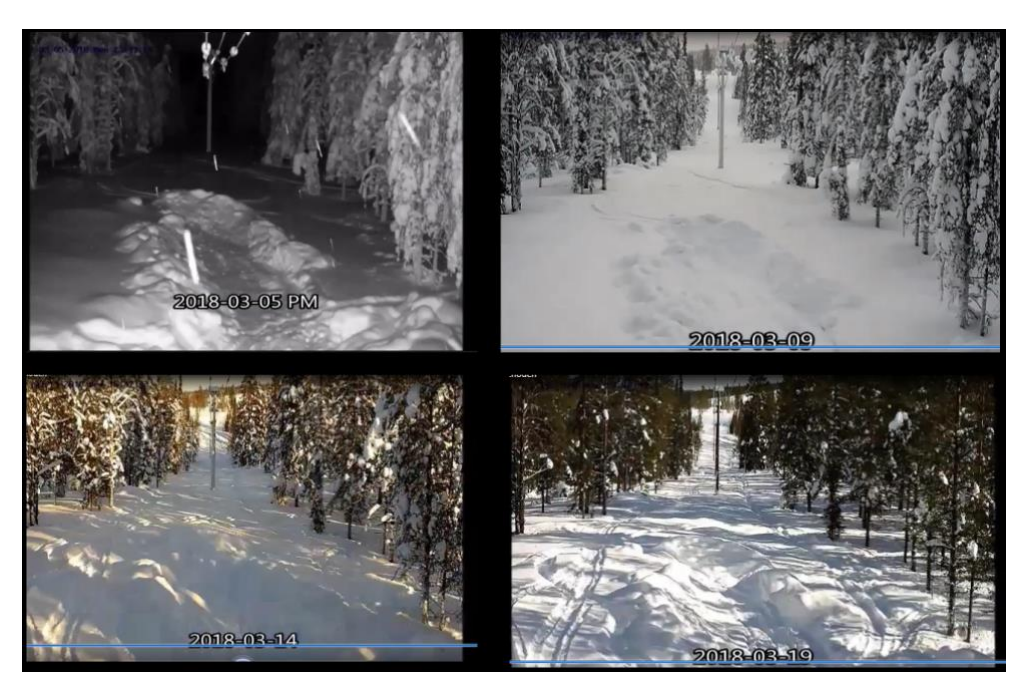


Figure 4-15: Four video stills taken from the recordings during Period 6 to illustrate major events

5 Discussion

The report explores the ongoing challenges and advancements in modeling ice and snow loads on power lines. By developing a higher resolution model, local terrain can be better represented, significantly impacting ice formation and resulting in a more reliable model. The ongoing work aims to develop a more accurate model tailored to Swedish conditions.

The comparison with over 100 wind speed measurements spread across Sweden, measured at 10 m height, showed that the wind speed in the model is generally too high compared to observations. However, the bias has decreased in the KVTMeso750 model compared to the KVTMeso1 model, with the greatest improvement seen in terrain classes 2, 3, and 4 (i.e., low vegetation, permanent forests, and villages/urban environments). This improvement is attributed to both higher resolution and updated model configuration, including different physical schemes for boundary layer meteorology used in the new model.

The analysis of the video recording indicates that wind reduction (a factor of 40% reduction was applied to account for sheltering in the forest) is necessary and has a significant impact. However, further studies and measurements are needed to refine this factor, including effects of the forest clearing on the wind field and its dependency on the wind direction relative to the line route. The video recording and model agree in many cases regarding ice buildup and snow shedding, but there are also instances of misalignment. The calculations are sensitive to model temperature, which significantly affects melting. The video recording confirms the stochastic nature of the snow shedding process, with almost always some snow and ice remaining on the lines after shedding events (partial shedding). The model, however, assumes the line is completely clean after melting periods, which is not always accurate. The difference between partial and complete shedding may significantly affect the further ice growth in subsequent snow fall episodes.

Incorporating turbulence into the icing model could enhance the accuracy of snow shedding predictions. Additionally, the model assumes the line has the same temperature as the surroundings, which is incorrect due to the joule heating occurring when electrical current flowing through the conductors.

Accurate measurements of wind and ice are crucial for calibrating the model for forested areas, which would lead to more reliable LineLoads calculations. All forms of data are valuable for ongoing work on the model and there are many different sensors available for monitoring ice loads. Ice and snow can also be collected and weighed, an informative instruction video has been published by Vattenfall Eldistribution to inspire more distribution companies to contribute to data collection. Further studies are needed to understand the differences in ice buildup and ice shedding on coated versus uncoated lines, as this difference remains significant.

Note that with the stochastic nature of the ice shedding process it will be impossible to reproduce individual icing events 1:1, even with a perfectly tuned icing model. Instead, the goal of future model calibrations is to obtain a modelling



system that reproduces the long-term statistical distribution of ice loads, and consequently reliable assessments of the extreme values (e.g. 50-year return period) for mapping and design purposes. Future data collection should therefore focus on establishment of systems for systematic and continuous measurements ice loads with a long-term perspective.

Another important question to address is the adequacy of current design practices for ice loads. Should network owners always consider actual vertical snow loads in forested areas when designing new lines? The high costs of meeting electrical distance requirements at maximum load in all locations are key, and not necessarily the most sustainable solution. A potential alternative could involve the use of monitoring systems to act faster when ice and snow are building up and manual removal is needed. Such solutions could also benefit from operational icing forecasts developed based on a calibrated LineLoads model.

Based on the findings of this report, further efforts are needed to create a reliable climatological power line icing map applicable for distribution lines. Such a map could ideally be used for design and planning, showing expected return values of extreme icing conditions in all of Sweden, including local icing phenomena in forested terrain.



6 Conclusion and recommendations

The key findings in this report include:

- Wind data comparison: Wind data from the new KVTMeso750 model was compared with measurements from over 100 SMHI stations across Sweden. The new model showed reduced bias, especially in terrain classes with low vegetation, permanent forests, and urban environments.
- Analysis of video recording: A video recording documenting weather
 conditions and loads on a distribution line segment in Northern Sweden
 during the winter of 2017-2018 was used for validation. The analysis
 highlighted the need for wind reduction factors and showed discrepancies
 in ice buildup and snow shedding predictions.
- Model sensitivity: The model's accuracy is sensitive to temperature, affecting melting predictions. The video recording showed that snow shedding is stochastic, while the model assumes complete shedding after melting periods.

These following recommendations aim to improve the reliability and operational forecasts of power lines under snow and ice loads, ensuring better preparedness and response to extreme weather conditions:

- Refine wind reduction factor: Conduct further studies to refine the wind reduction factor, especially in forested terrain. Also incorporating turbulence, wind gusts and directional effects to enhance model accuracy.
- 2. **Improve temperature sensitivity**: Enhance the model's sensitivity to temperature variations to better predict melting and snow shedding (probabilistic methods).
- 3. Expand data collection: Encourage more distribution companies to contribute to data collection, using sensors to monitor ice loads and collect snow and ice samples as accurate wind and ice measurements are crucial for calibrating the model.
- 4. **Develop climatological icing map**: Create a climatological power line icing map for Sweden to aid in design and planning, showing expected return values of extreme icing conditions.
- 5. **Evaluate coated vs. uncoated lines**: Perform studies on the differences in ice buildup and ice shedding on coated versus uncoated lines.



7 Bibliography

- Elíasson, Á. J., Hannesson, G. M., Ágústsson, H., & Þorsteins, E. (2019). Shedding of in-cloud icing. *IWAIS*. Reykjavik.
- Elíasson, Á., Hannesson, G., & Thorsteinson, E. (2017). Wet snow icing—Analysis of field measurements 1999–2016. *International Workshop on Atmospheric Icing of Structures*.
- (2012). EN 50341 1: Overhead electrical lines exceeding AC 1 kV Part 1: General requirements Common specifications.
- Finstad, K. J., Lozowski, E. P., & Gates, E. M. (1988). A computational investigation of water droplet trajectories. *Journal of atmospheric and oceanic technology*, *5*(1),, 160-170.
- Harstveit, K. (2009). Using metar-data to calculate in-cloud icing on a mountain site near by the airport. In , Andermatt, Switzerland. *WAIS*. Andermatt.
- Ingvaldsen, K., Nygaard, B. E., Byrkjedal, Ø., & Iversen, E. C. (2019). Validation of Modelled In-cloud Ice Accretion on Overhead Power Lines at Exposed High Altitude Sites in Norway. *IWAIS*.
- Liléo, S., Berge, E., Undheim, O., Klinkert, R., & Bredesen, R. (2013). Long-term correction of wind measurements. State-of-the-art, guidelines and future work. Elforsk.
- Makkonen, L. (1989). Estimation of wet snow accretion on structures. . *Cold Regions Science and Technology*, 17(1), 83-88.
- Makkonen, L. (2000). Models for the growth of rime, glaze, icicles and wet snow on structures. *Philosophical Transactions of the Royal Society of London.*Series A: Mathematical, Physical and Engineering Sciences, 358(1776),, 2913-2939.
- Nygaard, B. E., Ágústsson, H., & Somfalvi-Tóth, K. (2013). Modeling wet snow accretion on power lines: improvements to previous methods using 50 years of observations. *Journal of Applied Meteorology and Climatology*, 2189-2.
- Nygaard, B. E., Byrkjedal, Ø., Iversen, E., Fredbo, M., & Ágústsson, H. (2017).

 Development of a reliable modelling system for the calculation of rime ice loads on overhead transmission lines. *IWAIS*.
- Nygaard, B. E., Carlshem, L., Bartsch, J., Lee, L., & Ágústsson, H. (2019).

 Development of a 50-year return value ice load map for Sweden.

 International Workshop on Atmospheric Icing of Structures.
- Nygaard, B. E., Kristjánsson, J. E., & Makkonen, L. (2011). Prediction of in-cloud icing conditions at ground level using the WRF model. *Journal of Applied Meteorology and Climatology*, 2445-2459.
- Rasmussen, R. M., Geresdi, I., Thompson, G., Manning, K., & Karplus, E. (2002). Freezing drizzle formation in stably stratified layer clouds: The role of radiative cooling of cloud droplets, cloud condensation nuclei, and ice initiation. *Journal of the atmospheric sciences*, *59(4)*, 837-860.



- Roberge, M. (2005). The Physics of Wet Snow Accreted on an Overhead Wire. Structural Engineering Series Report no. 2005-03, 16.
- Sokolov, P., & Virk, M. S. (2019). Droplet distribution spectrum effects on dry ice growth on cylinders. *Cold Regions Science and Technology, 160*, 80-88.



Appendix A Description of the KVTMeso model

Three model simulations have been applied in this work, namely KVTMeso3, KVTMeso750 and KVTMeso1. The KVTMeso product is based on weather simulations applying the Weather Research and Forecast (WRF) model.

The WRF model is a state-of-the-art meso-scale numerical weather prediction system, aiming at both operational forecasting and atmospheric research needs. Numerous WRF simulations are performed at Kjeller Vindteknikk, covering different areas and time periods.

A detailed description of the modelling system can be found on the WRF home page¹. The development of the WRF-model is supported by a strong scientific and administrative community in the USA. The number of users is large, and the code is accessible to the public.

A.1 Model Setups

KVTMeso3 is simulated in $3 \text{ km} \times 3 \text{ km}$ horizontal resolution, covering the whole of Norway, Sweden and Finland. KVTMeso750 and KVTMeso1 covers Sweden and are simulated in horizontal resolutions of 750 m \times 750 m and 1 km \times 1 km, respectively.

While KVTMeso1 is divided into six subdomains, KVTMeso750 consists of only two domains, as shown in Figure A-7-1. KVTMeso3 domain covers the whole of Norway, Sweden and Finland and is not shown.



¹ https://www.mmm.ucar.edu/models/wrf

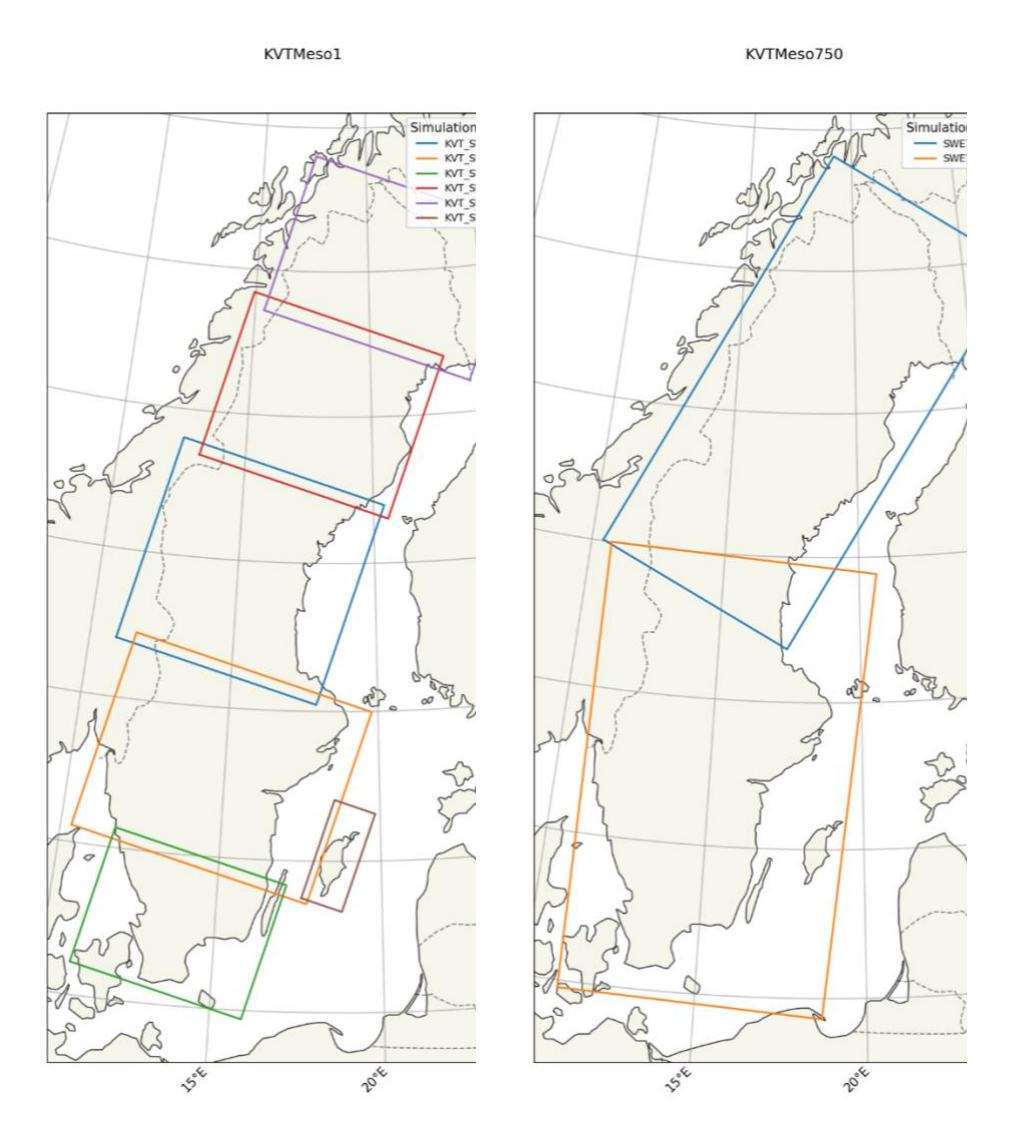


Figure A-7-1: The model domains of KVTMeso1 (left) and KVTMeso750 (right).

The simulations in KVTMeso3 utilise the WRF version 4.1.2 with improvements of wet snow behaviour documented by Iversen et al. (2021)² while KVTMeso1 uses the WRF version 3.2.1. The simulations are run with 32 layers in the vertical with four layers in the lower 200 m. The new KVTMeso750 utilise the WRF version 4.6.1 and is run with 51 vertical layers, where eight layers can be found in the lower 200 m. The physics schemes used are slightly different between datasets, summarised in Table A-1.

Energiforsk

42

 $^{^2}$ Emilie C. Iversen, Gregory Thompson and Bjørn Egil Nygaard, 2021: Improvements to melting snow behavior in a bulk microphysics scheme, Atmospheric Research, vol. 253, 105471, doi: 10.1016/j.atmosres.2021.105471

Table A-1: Overview of the simulations and physics schemes used in the KVTMeso3, KVTMeso750 and KVTMeso1.

| Description | KVTMeso3 | KVTMeso750 | KVTMeso1 |
|-----------------------|---|--|--|
| Version | 4.1.2 | 4.6.1 | 3.2.1 |
| Horizontal resolution | 3 km x 3 km | 750 m x 750 m | 1 km x 1 km |
| Vertical resolution | 32 layers | 51 layers | 32 layers |
| Boundary conditions | ERA5 + ERA5-Land | ERA5 | FNL |
| Simulation length | Full years September- August, one day spin- up disregarded. | Monthly simulations, one day spin-up | Daily simulations, 3 hours spin-up disregarded. |
| Spectral nudging | Yes | Yes | No |
| Microphysics | Thompson aerosol- aware microphysics | Thompson aerosol- aware microphysics | Thompson microphysics |
| Boundary layer | Mellor-Yamada Nakanishi and Niino (MYNN) Level 2.5 PBL | Mellor-Yamada Nakanishi and Niino (MYNN) Level 2.5 PBL | Yonsei University (YSU) |
| Surface layer | MYNN | MYNN | Monin-Obukhov |
| Land surface | Noah Land Surface Model | Noah Land Surface Model | Noah Land Surface Model* |
| Radiation | RRTMG | RRTMG | Dudhia |
| Simulation period | 1979-09-01 – 2025-02- 28 | 2017-11-01 – 2018-03- 31 and 2019-09-01 – 2020-08-31 | 2009-10-01 - 2011-04- 30 / 2009-10-01 - 2011-09- 30 / 2010-01-01 - 2010-12- 31 ** |

^{*}Except for the northernmost domain, where a 5-layer thermal diffusion scheme was used

As shown in Table A-1, the simulation period varies between the simulations, but the output is hourly.

A.2 Input data

The most important input data for the atmospheric model are geographical data and meteorological data. The geographical data is from National Oceanic and Atmospheric Administration (NOAA). The data includes topography, surface data, albedo and vegetation. These parameters have a high influence on the wind speed in the layers close to the ground. For KVTMeso1, surface roughness and landuse have been updated from Lantmäteriets GSD database. For KVTMeso3, the landuse dataset has been updated to the CORINE dataset. For KVTMeso750 terrain is based on Swedish digital terrain model in 50 m horizontal resolution (DTM50), with additional DTM50 data for Norway and Finland. KVTMeso750 landuse is taken from the CORINE dataset of 2018³.

Energiforsk

^{**}The two southernmost domains cover 2009-10-01 – 2011-09-30, while the Gotland simulation covers 2010-01-01-2010-12-31

³ CORINE 2018, V2020_20u1, doi: https://doi.org/10.2909/960998c1-1870-4e82-8051-6485205ebbac.

Atmospheric data from the European Center for Medium range Weather Forecasting (ECMWF) was used to force the model in KVTMeso3. The global reanalysis data ERA54 is available with a spatial resolution of approximately 30 km. The ERA5 dataset is constructed using an assimilation model that incorporates all relevant observational data across the globe, giving an updated description of the state of the atmosphere. The assimilation model incorporates data from several thousand ground-based weather stations, vertical profiles from radiosondes, aircrafts, and satellites. For surface variables like skin temperatures, soil temperatures and soil moisture, a special ERA5 dataset for land surface is applied, ERA5-Land. The dataset is based on the Carbon Hydrology-Tiled ECMWF Scheme for Surface Exchanges over Land (CHTESSEL). ERA5-Land is atmospherically forced by ERA5 and has even higher spatial resolution (0.1 degrees, ~9 km). The data is available with a temporal frequency of 1 hour, but for simulations each third hour is used for boundary conditions.

KVTMeso750 applies the ERA5 boundary conditions, whereas KVTMeso1 applies the FNL dataset. The FNL⁵ dataset is a global meteorological reanalysis dataset with 1 degree resolution, available from the National Centres for Environmental Protection (NCEP) with 6 hours interval. The data originates from the Final Global Data Assimilation System (FNL). FNL is an operational assimilation model that incorporates all available observation data globally and uses this data to create a global analysis dataset, or a snapshot of the atmosphere, four times every day, specifically at 00, 06, 12 and 18 UTC.

⁵ NCEP FNL dataset d083002, https://rda.ucar.edu/datasets/d083002/, doi: 10.5065/D6M043C6



⁴ https://confluence.ecmwf.int/display/CKB/ERA5

Appendix B Description of the icing calculations

Since icing is not a variable in the WRF model itself, it needs to be calculated as a post processing of the WRF model data. An icing model used for a continuous, long-term simulation of icing on conductors needs to include the following processes:

- <u>Ice accumulation.</u> The primary icing processes are rime icing (in-cloud icing), wet-snow icing and glaze icing (freezing rain).
- 2. <u>Ice persistence.</u>
- 3. <u>Ice removal.</u> The ice removal processes are sublimation, melting and ice shedding.

It is site-dependent which process is the most important when considering extreme icing. Icing models are often documented in detail for the accumulation part. However, the severity of icing in cold areas can be strongly influenced by ice removal processes, e.g. in situations with repeated accumulation of, rime ice occurring before a situation with ice removal. Extreme icing can, in some cases continue for days, weeks and even months.

Icing models are often applied without considering the actual span direction, named "omni" in this report. It generally should lead to overestimation since it accounts for accumulation from all directions without considering the icing particle's flux direction relative to the accumulating area. An example of such omni-directional model approach is the rime icing map for Sweden shown in (Nygaard, Carlshem, Bartsch, Lee, & Ágústsson, 2019).

For a particular power line when the actual span direction as well as the wind direction is known the icing particles flux is reduced/corrected when it is not perpendicular to the span. This is included in the model results presented in this report, however the omni-directional results are also presented in the same graphs.

Even though models for rime ice, wet snow and freezing rain often are described separately, the general approach is similar and can be described by equation (1). The model aims to simulate the icing process on the conductor from the start of accumulation until it disappears. The different terms on the right-hand side of (1) describe the rate of change of ice mass (dM/dt) due to rime icing from cloud droplets, wet snow accretion, dry snow accretion, freezing rain icing, sublimation, melting and shedding.

$$\begin{pmatrix} dM/_{dt} \end{pmatrix}_{Tot} = \begin{pmatrix} dm/_{dt} \end{pmatrix}_{Cloud} + \begin{pmatrix} dm/_{dt} \end{pmatrix}_{Wet\,snow} + \begin{pmatrix} dm/_{dt} \end{pmatrix}_{Dry\,snow} + \begin{pmatrix} dm/_{dt} \end{pmatrix}_{Rain} - \begin{pmatrix} dm/_{dt} \end{pmatrix}_{Sub} - \begin{pmatrix} dm/_{dt} \end{pmatrix}_{Melt} - \begin{pmatrix} dm/_{dt} \end{pmatrix}_{Shedding}$$
 (1)

Different approaches can be taken when applying (1) for icing modelling, either to include all accumulation terms in one simulation (a) or run separate simulations for the different icing types (b). If single icing events consist of a mixture of icing



types, (a) would give more realistic results, however to the author's experience such combined events are rare in nature and approach (b) normally gives similar results. In the current report we use a combination of the two approaches since we separate between rime ice and wet snow (approach (b)) while dry snow is included in both (approach (a)). All ice removal terms are included.

A basic approximation in many icing models is the cylindrical approximation. It is a well-studied model and is often referred to as the Makkonen model or the ISO12494 model. The main assumption of the cylindrical model is that the icing accumulates in the radial direction, so that the cylindrical geometry of the ice sleeve is maintained during the icing event. In reality, icing only occurs on the upstream (exposed) side of the conductor, however due to twisting of the conductor as well as ice sliding on the conductor's surface, observed icing on overhead lines are often well described as cylindrically shaped. For torsional rigid conductors (e.g. short spans of bundled conductors) the cylindrical assumption may lead to conservative ice loads.

The basic equation for ice accumulation of the cylindrical icing model is

$$\frac{dM}{dt} = \alpha_1 \cdot \alpha_2 \cdot \alpha_3 \cdot w \cdot V \cdot D \tag{2}$$

where

- *dM/dt* is the icing rate
- w is the mass concentration (kg/m³) of the icing particles in the air.
- α₁ is the collision efficiency. It describes if a particle hits the object through a collision.
- α is the sticking efficiency. It explains if a particle that hits an object will stick to it or bounce back.
- α3 is the accretion efficiency. It defines if a particle that sticks to an object will freeze or drip off as liquid water.
- *D* is the total diameter of the iced cylinder.
- *V* is the velocity of the particles perpendicular to the object [m/s]. The particle's velocity is the vector sum of the wind speed and the particle fall speed.

Time integration

A time step (dt) of one hour is used in the analysis. This corresponds to the temporal resolution of the WRF hindcast data. The time integration is performed in the following order:

1. Calculate ice mass *M* at time *i* using:



$$M_i = M_{i-1} + \left(\frac{dM}{dt}\right)_i \cdot dt \tag{3}$$

- 2. Update the total ice density ρ_i
- 3. Update the total icing diameter using:

$$D_{i} = \left[\frac{4(M_{i} - M_{i-1})}{\pi \rho_{i}} + D_{i-1}^{2} \right]^{1/2}$$
(4)

In the following sub-chapters the icing models for rime ice and wet snow are described in more details, including the list of variables from the WRF hindcast used as input for the different models.

B.1.1 Model for rime ice

Rime ice accumulation is calculated based on the cylindrical approximation, using the formulas from (Finstad, Lozowski, & Gates, 1988) and (Makkonen L., 2000). The model used for rime in this report includes the contribution from glaze ice caused by freezing rain/drizzle. The governing equation for the rime icing model used in this report thus becomes:

$$\left(\frac{dM}{dt} \right)_{Rime} = \left(\frac{dm}{dt} \right)_{Cloud} + \left(\frac{dm}{dt} \right)_{Rain} - \left(\frac{dm}{dt} \right)_{Sub} - \left(\frac{dm}{dt} \right)_{Melt}$$
 (5)

A list of WRF variables used as input to the rime icing model is given in Table B-1

Table B-1: List of meteorological variables used in the rime icing model.

| Variable | Unit | Description |
|-----------------------|-------------|--|
| Wind speed | m/s | Horizontal wind speed |
| Wind direction | Deg (0-360) | |
| Air Temperature | K | Normally extracted at the lowest vertical level of WRF |
| Specific air humidity | g/kg | |
| Air pressure | Pa | |
| Q_{cloud} | kg/m³ | Mass concentration of cloud liquid water |
| Q _{rain} | kg/m³ | Mass concentration of rain/drizzle liquid water |
| SWDOWN | W/m_2 | Incoming short-wave radiation |



Efficiency coefficients

The collision efficiency α_1 is an essential part of the rime icing model. For cloud droplets we calculate α_1 according to (Finstad, Lozowski, & Gates, 1988), based on the wind speed, icing diameter and the median volume cloud droplet diameter (MVD). We diagnose the MVD from the WRF output according to the equations in (Nygaard, Kristjánsson, & Makkonen, Prediction of in-cloud icing conditions at ground level using the WRF model, 2011).

Traditionally, the MVD approach has been widely used for calculation of the collision efficiency between droplets and a cylinder. There are, however, limitations of the MVD approach which is particularly important for large icing diameters typically occurring in rime ice conditions at exposed sites ((Nygaard, Byrkjedal, Iversen, Fredbo, & Ágústsson, 2017), (Ingvaldsen, Nygaard, Byrkjedal, & Iversen, 2019) and (Sokolov & Virk, 2019)). In the current model we have replaced the MVD with a full droplet size distribution and calculated the collision efficiency for each bin of the distribution. Various droplet size distributions (referred to as "Langmuir distributions") have been implemented as options in the model, based on the set of different distributions as shown in Table B- 2. The numbers in the table represent the ratio of the droplet diameter in the various bins to the MVD. An example of the Langmuir D distribution is shown visually in Figure B-1.

Table B- 2: Langmuir droplet size distributions. The numbers represent the droplet diameter ratios for the various bins of the distributions

| LWC fraction | A | В | C | D | E | F | G | Н | J |
|--------------|------|------|------|------|------|------|------|------|------|
| 0.05 | 1.00 | 0.56 | 0.42 | 0.31 | 0.23 | 0.18 | 0.13 | 0.10 | 0.06 |
| 0.1 | 1.00 | 0.72 | 0.61 | 0.52 | 0.44 | 0.37 | 0.32 | 0.27 | 0.19 |
| 0.2 | 1.00 | 0.84 | 0.77 | 0.71 | 0.65 | 0.59 | 0.54 | 0.50 | 0.42 |
| 0.3 | 1.00 | 1.00 | 1.00 | 1.00 | 1.00 | 1.00 | 1.00 | 1.00 | 1.00 |
| 0.2 | 1.00 | 1.17 | 1.26 | 1.37 | 1.48 | 1.60 | 1.73 | 1.88 | 2.20 |
| 0.1 | 1.00 | 1.32 | 1.51 | 1.74 | 2.00 | 2.30 | 2.64 | 3.03 | 4.00 |
| 0.05 | 1.00 | 1.49 | 1.81 | 2.22 | 2.71 | 3.31 | 4.04 | 4.93 | 7.34 |

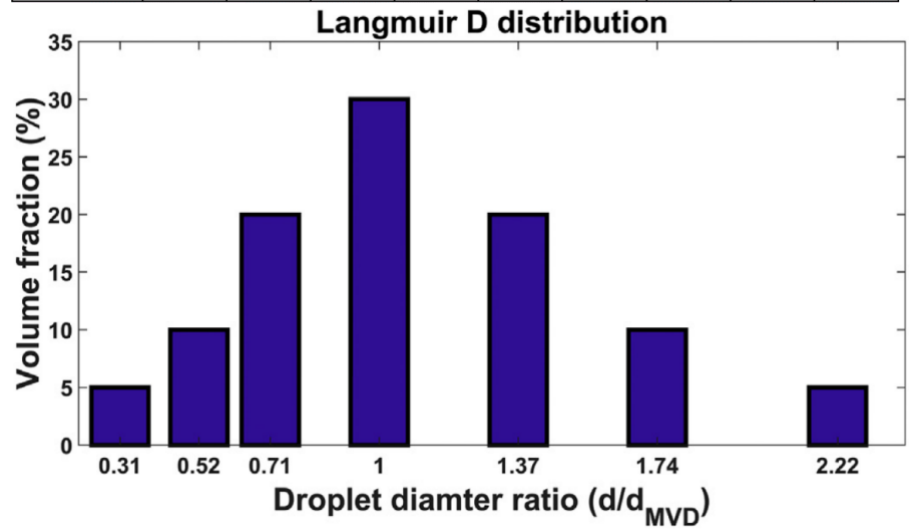




Figure B-1: Langmuir D droplet size distribution

In cases of high cloud LWC (liquid water content) the supercooled clouds may start to produce larger droplets, known as freezing drizzle. Such droplets typically have an MVD of 100 μ m which implies a high collision efficiency of approximately 90 % with a reference cylinder, compared to about 10 % for a typical cloud droplet with MVD in the range 10 – 20 μ m. Therefore, even at low mass concentrations, any freezing rain or drizzle in the air may contribute significantly to the total ice accumulation, with almost 10 times the collision efficiency of cloud droplets. In clean arctic air the likelihood of freezing drizzle is high due to a low cloud droplet number concentration, and the rapid growth of cloud to drizzle size droplets (Rasmussen, Geresdi, Thompson, Manning, & Karplus, 2002).

The details of the rime icing model are described in (Makkonen L. , 2000), including equations for calculation of the collision efficiency (α_1) of cloud droplets with cylinders, as well as the accretion efficiency (α_3) which accounts for the effect of latent heat release on the ice surface. The formulas used for the accretion efficiency (α_3) in the rime icing model are identical to the ones in (Makkonen L. , 2000).

The sticking efficiency α_2 is assumed to be 1 for supercooled droplets hitting an object.

Melting and sublimation

Two processes responsible for reduction of ice mass are implemented in the model. These are melting and sublimation. Melting takes place when there is a positive energy balance on the ice surface whereas sublimation takes place when the air is sub-saturated with respect to ice. Both processes have increasing rates with increasing wind speed, and the orientation of the conductor relative to the wind affects the melting and sublimation rates.

Ice melting is calculated by evaluating the energy balance model, given by

$$Q_{\text{melt}} = Q_h + Q_e + Q_n \tag{6}$$

where Q_h and Q_e are the sensible and latent heat fluxes. Q_n is the net radiation term. There are also other terms which will come into the total energy balance model, however they are of negligible size in this context. The term Q_{melt} in equation (6) is then the heat flux available to melt the ice. The melted ice mass (dM_{melt}) each time step in the model is found by

dM_{melt}=Q_{melt} /Lf

(7)



where L_f is the heat of fusion/melting ($L_f = 3.34 * 10^5 \text{ J/kg}$). More details on the energy balance model is given in (Harstveit, 2009).

Sublimation is calculated in the same manner, based on the energy balance. During sublimation the evaporative heat flux is balanced by the sensible heat flux and radiative heat flux.

$$Q_e = -(Q_h + Q_n) \tag{8}$$

In such conditions the surface temperature of the ice will be different from the air temperature, and the energy balance is solved numerically by iteration. Once the iteration has converged the sublimated mass dM_{sub} each time step is found by

$$dM_{sub}=Q_e/Ls$$
 (9)

where L_s is the heat of sublimation ($L_s = 2.82 * 10^6 J/kg$).

Experience has shown that the actual rates of reduction in ice mass during sublimation and melting are higher than the theoretical rates from the energy balance model. This has led to the introduction of shedding factors, to account for the mechanical loss of mass through e.g. parts of the accreted ice falling off. These are empirical factors that increase the melting and sublimation rates. In the current model the shedding factor for melting and sublimation are 3.5 and 1.15 respectively.

These factors have been optimized with respect to observed melting and sublimation rates on a test span at an exposed rime ice site in Norway (Ingvaldsen, Nygaard, Byrkjedal, & Iversen, 2019). The calibration of the shedding factors was based on three winter seasons worth of data (approximately a total of 20 melting episodes and 10 prolonged sublimation episodes, one of which lasted for almost six weeks).

Spontaneous shedding

Provided meteorological input data of sufficient quality, the rates at which rime ice accumulates, melts and sublimates on overhead power lines can be calculated deterministically with relatively high precision using current icing models (Ingvaldsen, Nygaard, Byrkjedal, & Iversen, 2019). However, even if the accumulation, melting and sublimation rates are captured perfectly, the ice accretion model will overestimate the long-term extreme values unless it also



accounts for spontaneous ice shedding. This is particularly true when the model is used to predict ice accumulation on bundle conductors or other conductor configurations with high rotational stiffness on which ice will typically form as "ice vanes" on the windward side, compared to e.g. a thin earth wire which will allow for a more robust, cylindrical ice growth due to conductor rotation during icing.

Spontaneous shedding is a stochastic process and therefore inherently difficult to model deterministically (Elíasson Á. J., Hannesson, Ágústsson, & Þorsteins, 2019). In the ongoing research project ICEBOX 6 , we aim to develop a probabilistic ice shedding model based on long records of test span measurements on Iceland. However, the results are preliminary at this point and the shedding model needs to be properly validated before it can be applied to extreme value calculations.

Assumptions in the rime icing model

The following list summarizes the main assumptions of the rime icing model:

Table B-3: List of main assumptions in the model used for rime ice

| Variable/parameter | Assumption |
|--|--|
| Icing criteria | lce growth is only considered at temperature (T) < 0° C and requires the presence of cloud droplets and/or rain droplets. |
| The collision coefficient α_1 for cloud droplets | Calculated using the Langmuir J size distribution. |
| Lower limit for α_1 | We limit α_1 by limiting the Stokes number K=max(K , 0.25) |
| The collision coefficient α_{1} for rain and drizzle | assumed equal to 0.9. |
| Sticking coefficient α_2 | Assumed equal to 1. |
| The accretion coefficient α_3 | Calculated every time step based on the energy balance on the ice surface, considering accretion from both cloud water and rain. |
| Sublimation rate | Solved numerically every time step using the energy balance equation (7). |
| Melting rate | Calculated every time step using the energy balance equation (9). |
| Ice shedding during melting and sublimation | Sublimation and melting rates are scaled with empirical factors (shedding factors) SF _{sub} =1.15, SF _{melt} = 3.5 |
| Spontaneous ice shedding | Not included in the model |
| Density of rime | Calculated every time step using the approach described in (Makkonen L., 2000). |
| Density of Glaze | Calculated every time step using the approach described in (Makkonen L. , 2000) . |
| Total ice density | Calculated every time step as the mass weighted average of the contribution from cloud droplets and rain droplets. |
| Ice shape | Assumed cylindrical throughout the whole event. |
| Conductor diameter | Input parameter to the model. 30 mm used in this report. |
| Conductor torsional stiffness | Assumed to be 0. I.e., a freely rotating conductor. |
| Conductor temperature | Assumed equal to ambient temperature. Joule heating is not included. |

⁶ https://www.statnett.no/en/about-statnett/research-and-development/our-prioritised-projects/icebox/



51

| Variable/parameter | | | Assumption | |
|--------------------|--------|-------|---|--|
| Conductor ground | height | above | Input parameter to the model. 15 m used in this report. | |
| Span direction | | | Input parameter to the model. Different for each site studied in this report. | |

B.1.2 Model for snow accretion

Wet snow occurs during snow fall at temperatures just above freezing. Snow particles falling from colder air aloft start to melt when entering warmer air closer to the ground. The vertical distance in which the melting of snowflakes occurs is called the melting layer of the atmosphere, and wet snow accretion may take place when a structure (e.g. a power line) is located within the melting layer Figure B-2. Snow particles that contain a certain amount of liquid water will become sticky, enabling the particles to accrete on almost any type of object.

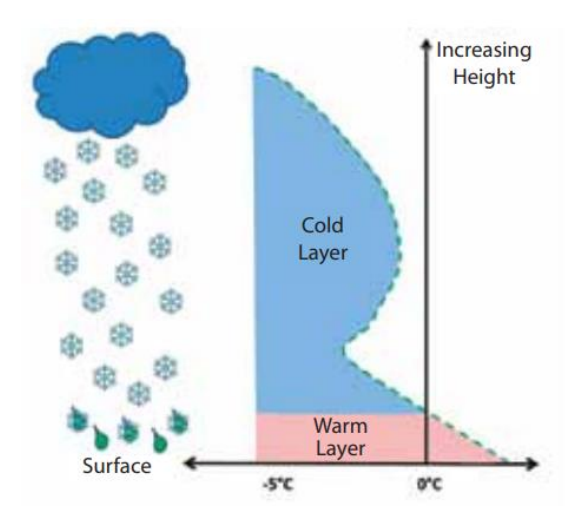


Figure B-2: Conceptual figure showing a typical temperature profile during wet snow events, with a melting layer close to the ground.

Wet snow accumulation rates can be modelled based on precipitation, wind, temperature and humidity data. In particular, the effectiveness of which wet snowflakes stick to objects such as overhead power lines is highly sensitive to the wet-bulb temperature, Tw. As opposed to the dry-bulb temperature (normally referred to as air temperature), the wet-bulb temperature also accounts for evaporative cooling and is thus related to the relative humidity. In short, a snowflake in thermodynamic balance with its environment may contain liquid water only if the wet-bulb temperature is above 0 °C (Makkonen L. , 1989).

The accumulation model applied in the present analysis calculates wet snow accumulation using the cylindrical model approximation and is described in detail in (Nygaard, Ágústsson, & Somfalvi-Tóth, 2013). The model is calibrated against a large dataset from Iceland consisting of icing observations on operational lines, load cell measurements in operational lines as well as load cell measurements in test spans (Elíasson, Hannesson, & Thorsteinson, 2017). In addition to



accumulation of wet and dry snow, the model includes sublimation and melting. The governing equation for the snow accretion model used in this report is:

The necessary meteorological variables listed in are extracted as hourly time series from WRF and used as input to the snow accretion model.

Table B-4: List of meteorological variables used in the snow accretion model

| Variable | Unit | Description |
|---------------------------|-------------|---|
| Wind speed | m/s | Horizontal wind speed |
| Wind direction | Deg (0-360) | |
| Air Temperature | K | Extracted at the lowest vertical level of WRF |
| Specific air humidity | g/kg | |
| Air pressure | Pa | |
| Hourly precipitation rate | mm/h | |
| Q_{cloud} | kg/m³ | Mass concentration of cloud liquid water |
| Q_{snow} | kg/m³ | Mass concentration of snow |
| Q_{rain} | kg/m³ | Mass concentration of rain |
| Q_{graup} | kg/m³ | Mass concentration of graupel |
| SWDOWN | W/m^2 | Incoming short-wave radiation |

Dry snow accretion

Dry snow particles may also accumulate on overhead power lines under certain conditions. The criteria for dry snow accumulation are less known, however, studies have shown that dry snow particles tend to bounce off overhead power lines at wind speeds exceeding 2-3 m/s (Roberge, 2005). Our current ice accretion model allows for dry snow accumulation at wind speeds up to 5-6 m/s, however, the fraction of dry snow particles that contributes to the ice load is significantly reduced at wind speeds exceeding 2-3 m/s. Another precondition for dry snow accumulation is that the conductor is already covered by ice due to riming or wet snow accretion (dry snow particles tend to bounce off bare conductors, even at lower wind speeds than 2-3 m/s).

Melting and sublimation

Sublimation is calculated with the same code as used in the rime icing model, as described in Chapter B.1.1.

Melting, is however somewhat different between snow accretion and rime ice. During wet snow icing, meltwater on the ice deposit surface tends to infiltrate the snow sleeve, due to the capillary forces. Normally melting takes place until the



snow sleeve reaches a critical liquid water fraction. At approximately 50% liquid water the cohesive forces in the snow will collapse, and complete shedding is observed. In the current model this is simplified to the assumption that all ice is removed by shedding if the wet-bulb temperature exceeds 1.5° C as an integrated value during a melting event. E.g. accreted snow can shed off if $T_{\rm w}$ exceeds 0.5° C during three consecutive hours, or $T_{\rm w}$ exceeds 1.5° C for one hour.

Assumptions in the wet snow icing model

The following list summarizes the main assumptions of the wet snow icing model:

Table B-5: List of main assumptions in the model used for wet snow

| Table B-5: List of main assumptions in the | e moder used for wet snow | | |
|--|--|--|--|
| Variable/parameter | Assumption | | |
| Temperature criteria | $T_w > 0$ | | |
| *Precipitation intensity criteria | A certain precipitation intensity is required in order to initiate wet snow accumulation on power lines. The criteria is derived from the energy balance equation. | | |
| | $Q_{\text{precip}} > \text{pi.*}(T_w).*\text{h.}$ / (Lf .* SR .* U .* α_2), where Q_{precip} is the total mass concentration of precipitation particles, h is the convective heat transfer coefficient, L_f is the latent heat of fusion, SR is the frozen fraction of the precipitation, U is the horizontal wind speed. | | |
| Dry snow criteria | Dry snow may accumulate when: 1. Pre-existing snow sleeve on the conductor 2. U < 5 m/s | | |
| The collision coefficient α_{1} for snow | Calculated as for rime but assuming an equivalent droplet MVD of 0.322 mm as a fixed value. | | |
| Sticking coefficient α_2 | $\alpha_2 = \frac{1 - \cos{(9 \cdot SR - 4.5)}}{2 \cdot U^{0.4}}$ when 0.5 < SR < 0.98, otherwise α_2 = 0. | | |
| *Graupel restriction of α_2 | The sticking coefficient is reduced as a function of the graupel amount, if graupel is present during wet snow conditions. | | |
| The accretion coefficient α_3 | α ₃ =1 | | |
| Sublimation rate | Similar as for rime ice. | | |
| Melting rate | Shedding when time integral of T _w > 1.5 | | |
| *Shedding | Complete shedding is assumed based on a combined criteria on ice density and wind speed: | | |
| | $U > 40*(\rho*001)$ and $\rho < 400$ | | |
| Density of wet snow | Calculated every time step using $\rho_{wetsnow}$ =200 + 25*U | | |
| Density of dry snow | Calculated every time step using $\rho_{drysnow}$ =100 + 20 *U | | |



| Variable/parameter | Assumption |
|-------------------------------|---|
| Total ice density | Calculated every time step as the mass weighted average of the contribution from wet snow and dry snow. |
| Ice shape | Assumed cylindrical throughout the whole event |
| Terminal velocity of wet snow | W _{wetsnow} = -0.000223 * (SR* 100) ² + 0.003276 * (SR * 100) + 3.108303 |
| Terminal velocity of dry snow | $W_{drysnows} = 1 \text{ m/s}$ |
| Conductor diameter | Input parameter to the model. 30 mm used in this report. |
| Conductor torsional stiffness | Assumed to be 0. I.e. a freely rotating conductor. |
| Conductor temperature | Assumed equal to ambient temperature. Joule heating is not included. |



Pite-Rönnskär BörtnamHunge Fännäs Klövsjöhöjdemorpsha ora Sp<mark>an</mark>sberget Kerst<mark>in</mark>bo Naven Kettstaka norra Östergarnsholm Hoburg

Appendix C Validation using SMHI observations

Figure C-1. Locations of SMHI observations used for the validation. The colours represent the different terrain categories. Light green: terrain category 0, dark green: terrain category 1, yellow: terrain category 2, red: terrain category 3 and orange: terrain category 4.



Table C-1 Results from synthesized modelled time series, comparing with 10 m wind speed observations at SMHI stations in the overlapping period 1979-2024 (October to May each year)

| Site | Bias | Bias | RMSE | RMSE |
|---------------|-------------|-------------|-------------|-------------|
| | KVTMeso750 | KVTMeso1 | KVTMeso750 | KVTMeso1 |
| | model [m/s] | model [m/s] | model [m/s] | model [m/s] |
| Abisko | -0.71 | -0.28 | 3.01 | 2.98 |
| Adelsö | 1.17 | 1.48 | 2.10 | 2.20 |
| Arjeplog | 1.55 | 1.88 | 2.29 | 2.67 |
| Arvidsjaur | 0.54 | 0.73 | 1.88 | 1.95 |
| Arvika | 0.99 | 2.19 | 1.88 | 2.88 |
| Bjuröklubb | -0.25 | -0.53 | 2.37 | 2.37 |
| Blåhammaren | -0.67 | -2.07 | 3.66 | 3.95 |
| Blomskog | 1.83 | 2.59 | 2.43 | 3.11 |
| Brämön | -0.11 | 0.55 | 2.25 | 2.39 |
| Buresjön | 0.60 | 1.24 | 1.73 | 2.19 |
| Börtnan | 0.94 | 1.41 | 1.94 | 2.44 |
| Daglösen | 1.35 | 2.05 | 2.06 | 2.67 |
| Delsbo | 1.10 | 1.82 | 1.96 | 2.64 |
| Dravagen | 0.59 | 1.17 | 1.81 | 2.27 |
| Edsbyn | 0.94 | 1.66 | 1.74 | 2.42 |
| Eggegrund | 0.90 | 0.84 | 2.47 | 2.52 |
| Eskilstuna | 0.74 | 1.33 | 1.87 | 2.20 |
| Falsterbo | 0.69 | 0.64 | 2.42 | 2.28 |
| Film | 1.54 | 2.60 | 2.19 | 3.10 |
| Floda | 0.63 | 1.80 | 1.76 | 2.52 |
| Fredrika | 1.24 | 1.81 | 1.93 | 2.55 |
| Fårösund | 0.25 | -0.11 | 2.14 | 2.22 |
| Föllinge | 0.85 | 0.92 | 1.96 | 1.96 |
| Gielas | 0.82 | 1.32 | 1.91 | 2.28 |
| Gladhammar | 0.92 | 1.92 | 1.77 | 2.53 |
| Gotska Sandön | 0.84 | 1.54 | 2.10 | 2.68 |
| Gubbhögen | 1.09 | 1.61 | 1.97 | 2.55 |
| Gunnarn | 1.08 | 1.33 | 2.02 | 2.29 |
| Gustavsfors | 1.00 | 2.08 | 1.82 | 2.68 |
| Gårdsjo | 1.55 | 1.85 | 2.19 | 2.36 |
| Gäddede | 2.26 | 2.27 | 3.26 | 3.09 |
| Gällivare | 1.08 | 1.06 | 2.18 | 1.88 |
| Gävle | 0.49 | 1.19 | 1.57 | 1.99 |
| Göteborg | 0.90 | 1.08 | 1.81 | 1.78 |
| Hallhaxåsen | 1.24 | 1.77 | 1.94 | 2.52 |
| Hamra | 1.53 | 1.74 | 2.14 | 2.45 |
| Hanö | -1.16 | -0.81 | 2.56 | 2.37 |
| Haparanda | 1.38 | 2.18 | 2.11 | 3.17 |
| Harstena | 2.25 | 1.29 | 3.03 | 2.20 |



| Site | Bias | Bias | RMSE | RMSE |
|--------------------------|-------------|-------------|-------------|-------------|
| | KVTMeso750 | KVTMeso1 | KVTMeso750 | KVTMeso1 |
| | model [m/s] | model [m/s] | model [m/s] | model [m/s] |
| Helsingborg | 0.88 | 1.45 | 1.83 | 2.19 |
| Hemavan- | -0.84 | -1.60 | 3.12 | 3.44 |
| Gierevarto | | | | |
| Hemling | 0.93 | 1.74 | 1.91 | 2.58 |
| Hoburg | 0.40 | 0.72 | 1.92 | 2.20 |
| Holmön | 1.26 | 0.97 | 2.75 | 2.63 |
| Horn | 0.37 | 1.52 | 1.68 | 2.27 |
| Hoting | 1.36 | 1.75 | 2.14 | 2.68 |
| Hunge | 1.07 | 1.70 | 2.01 | 2.49 |
| Hällum | 0.91 | 1.91 | 2.07 | 2.68 |
| Junsele | 1.36 | 2.15 | 1.90 | 2.78 |
| Järnasklubb | 0.98 | 1.08 | 2.35 | 2.57 |
| Karesuando | 0.56 | 0.60 | 1.64 | 1.61 |
| Katterjåkk | 0.93 | 0.08 | 3.66 | 2.86 |
| Kerstinbo | 1.35 | 1.96 | 2.21 | 2.53 |
| Kettstaka | 1.61 | 1.52 | 2.28 | 2.10 |
| Kilsbergen | 1.50 | 1.71 | 2.16 | 2.32 |
| Kloten | 2.28 | 2.18 | 2.93 | 2.72 |
| Klovsjöhöjden | 1.12 | 0.64 | 2.38 | 2.09 |
| Kolmården | 1.46 | 1.84 | 2.01 | 2.32 |
| Korsvattnet | 0.23 | -0.26 | 2.56 | 2.25 |
| Krångede | 1.07 | 1.55 | 1.98 | 2.58 |
| Kroppefjall-Granan | 2.14 | 2.62 | 2.78 | 3.11 |
| Kuggören | 0.50 | 0.74 | 2.30 | 2.46 |
| Kvikkjokk- Årrenjarka | 0.77 | 1.32 | 2.00 | 2.25 |
| Lakaträsk | 1.27 | 1.71 | 2.08 | 2.36 |
| Landsort | 0.85 | 0.49 | 2.53 | 2.41 |
| Latnivaara | 0.75 | 1.17 | 1.93 | 2.17 |
| Ljungby | 1.22 | 1.88 | 1.90 | 2.41 |
| Lungö | -0.15 | 0.24 | 2.60 | 2.69 |
| Lycksele | 0.41 | 1.08 | 1.75 | 2.31 |
| Malexander | 1.35 | 1.77 | 1.97 | 2.28 |
| Malå-Brännan | 1.37 | 1.75 | 2.21 | 2.47 |
| Malmö | 1.28 | 1.39 | 2.17 | 2.12 |
| Malung | 0.33 | 1.08 | 1.72 | 1.96 |
| Mierkenis | 1.37 | 0.89 | 2.88 | 2.22 |
| Mora | 0.22 | 1.11 | 1.56 | 2.07 |
| Målilla | 0.44 | 1.16 | 1.60 | 1.93 |
| Måseskar | 0.04 | 0.18 | 2.30 | 2.25 |
| Naimakka | 0.04 | 0.29 | 1.82 | 1.87 |



| Site | Bias | Bias | RMSE | RMSE |
|---------------------|-------------|-------------|-------------|-------------|
| | KVTMeso750 | KVTMeso1 | KVTMeso750 | KVTMeso1 |
| | model [m/s] | model [m/s] | model [m/s] | model [m/s] |
| Nattavaara | 1.15 | 1.58 | 2.08 | 2.36 |
| Naven | 1.78 | 2.57 | 2.68 | 3.40 |
| Nidingen | 0.16 | 0.35 | 2.26 | 2.30 |
| Nikkaluokta | 0.51 | 0.48 | 2.48 | 2.29 |
| Nordkoster | 0.48 | 0.46 | 2.15 | 2.16 |
| Norrköping-SMHI | 1.52 | 1.87 | 2.09 | 2.38 |
| Norsjö | 1.65 | 1.54 | 2.28 | 2.30 |
| Paharova | 1.37 | 1.56 | 2.09 | 2.19 |
| Pajala | 0.60 | 0.93 | 1.56 | 1.75 |
| Parkalompolo | 1.13 | 1.44 | 2.09 | 2.25 |
| Petisträsk | 1.65 | 2.49 | 2.34 | 3.16 |
| Pite-Rönnskar | 0.52 | 0.48 | 2.37 | 2.35 |
| Pålgrunden | -0.33 | -0.03 | 2.19 | 2.21 |
| Rensjön | -0.08 | 0.15 | 2.13 | 2.15 |
| Ritsem | 1.15 | 1.51 | 3.32 | 3.03 |
| Rångedala | 1.74 | 2.05 | 2.34 | 2.54 |
| Rödkallen | 0.54 | 0.62 | 2.42 | 2.53 |
| Saittarova | 0.78 | 0.66 | 1.81 | 1.61 |
| Sala | 1.35 | 2.46 | 2.27 | 3.24 |
| Skagsudde | 0.44 | 1.09 | 2.21 | 2.60 |
| Skarpö | 1.44 | 1.90 | 2.24 | 2.56 |
| Skillinge | 1.16 | 1.48 | 2.48 | 2.70 |
| Stekenjokk | -2.24 | -3.22 | 4.32 | 4.97 |
| Stora Sjöfallet | -0.23 | -0.74 | 4.09 | 4.08 |
| Stora Spånsberget | 1.91 | 2.14 | 2.66 | 2.80 |
| Storlien-Storvallen | 1.93 | 1.79 | 3.44 | 2.82 |
| Sunne | 0.88 | 1.80 | 1.85 | 2.55 |
| Svanberga | 2.57 | 2.81 | 3.25 | 3.35 |
| Sveg | 0.27 | 0.76 | 1.63 | 2.02 |
| Sylarna | 0.49 | -0.46 | 3.35 | 3.28 |
| Söderarm | -0.31 | -0.33 | 2.66 | 2.68 |
| Tarfala | 1.82 | 1.40 | 3.79 | 3.28 |
| Tomtabacken | 1.49 | 1.74 | 2.08 | 2.28 |
| Torpshammar | 1.54 | 2.05 | 2.17 | 2.70 |
| Torup | 0.45 | 1.28 | 1.46 | 1.94 |
| Tullinge | 0.43 | 1.18 | 1.72 | 2.04 |
| Tännas | 1.88 | 2.47 | 2.79 | 3.32 |
| Ullared | 2.44 | 3.15 | 2.97 | 3.59 |
| Uppsala | 1.47 | 1.90 | 2.05 | 2.43 |
| Utklippan | 0.59 | 0.64 | 2.41 | 2.42 |
| Väderöarna | -0.47 | -0.53 | 2.45 | 2.41 |



| Site | Bias KVTMeso750 model [m/s] | Bias KVTMeso1 model [m/s] | RMSE KVTMeso750 model [m/s] | RMSE KVTMeso1 model [m/s] |
|--------------------|-----------------------------------|---------------------------------|-----------------------------------|---------------------------------|
| Västmarkum | 1.19 | 2.06 | 2.09 | 2.80 |
| Växjo | 0.79 | 0.92 | 1.64 | 1.66 |
| Vilhelmina | 0.39 | 1.09 | 1.73 | 2.22 |
| Visingsö | -0.18 | 0.38 | 1.93 | 2.01 |
| Ylinenjarvi | 0.58 | 0.92 | 1.87 | 2.03 |
| Åmot | 0.51 | 1.43 | 1.79 | 2.34 |
| Åsele | 1.53 | 2.20 | 2.27 | 3.00 |
| Älvdalen | 0.24 | 1.24 | 1.58 | 2.18 |
| Älvsbyn | 0.39 | 1.08 | 1.64 | 2.12 |
| Ölands norra udde | 0.87 | 0.71 | 2.54 | 2.39 |
| Ölands södra udde | 0.71 | 0.96 | 2.43 | 2.54 |
| Östergarnsholm | 0.53 | 0.12 | 2.26 | 2.22 |
| Överkalix-Svartbyn | 1.58 | 1.71 | 2.26 | 2.38 |



ICETOOLS

This project aims to improve predictions of snow and ice loads on power lines in Sweden. A high-resolution model was developed to better represent local terrain and meteorological variability. Validation using SMHI wind data showed improved accuracy compared to previous model, especially in forested areas. In a case study, using video recordings from Vattenfall Eldistribution from a site in Northern Sweden, modeled icing was directly compared to actual icing. The comparison gave valuable understanding of the performance and limitations of the model, especially with regards to ice growth and shedding. It also highlighted the importance of including a wind reduction factor in forested terrain and revealed the model's sensitivity to temperature, identified as the main driver of snow shedding events. For a more robust statistical calibration and further development of the model, more direct measurements of icing and meteorological data are of high importance.

A new step in energy research

The research company Energiforsk initiates, coordinates, and conducts energy research and analyses, as well as communicates knowledge in favor of a robust and sustainable energy system. We are a politically neutral limited company that reinvests our profit in more research. Our owners are industry organisations Swedenergy and the Swedish Gas Association, the Swedish TSO Svenska kraftnät, and the gas and energy company Nordion Energi.

